Title

Counteracting Genome Instability by p53-dependent Mintosis

Authors

Jianqing Liang[1,6#], Zubiao Niu[1#], Xiaochen Yu[1#], Bo Zhang[1,2], You Zheng[1], Manna Wang[1,4], Banzhan Ruan[1], Hongquan Qin[1,4], Xin Zhang[1], Songzhi Gu[1], Xiaoyong Sai[3], Yanhong Tai[5], Lihua Gao[1], Li Ma[4], Zhaolie Chen[1], Hongyan Huang[2*], Xiaoning Wang[3*], Qiang Sun[1*]

Affiliations

[1]*Laboratory of Cell Engineering, Institute of Biotechnology, 20 Dongda Street, Beijing 100071, P.R. China.*
[2]*Department of Oncology, Beijing Shijitan Hospital of Capital Medical University, 10 TIEYI Road, Beijing 100038, P. R. China;*
[3]*National Clinic Center of Geriatric & the State Key Laboratory of Kidney, the Chinese PLA General Hospital, Beijing 100853, P.R.China*
[4]*Institute of Molecular Immunology, Southern Medical University, Guangzhou 510515, P. R. China*
[5]*The 307 Hospital, 8 Dongda Street, Beijing 100071, P. R. China*
[6]*State Key Laboratory of Genetic Engineering, School of Life Science, 2005,Songhu Road, Fudan University, Shanghai, 200438, People's Republic of China.*

*Correspondence to:

Qiang Sun
Email: sunq@bmi.ac.cn

Xiaoning Wang
Email: xnwang88@163.com

Hongyan Huang
Email: hhongy1999@126.com

[#] These authors contributed equally to this work

Abstract

Entosis was proposed to promote aneuploidy and genome instability by cell-in-cell mediated engulfment in tumor cells. We reported here, in epithelial cells, that entosis coupled with mitotic arrest functions to counteract genome instability by targeting aneuploid mitotic progenies for engulfment and elimination. We found that the formation of cell-in-cell structures associated with prolonged mitosis, which was sufficient to induce entosis. This process was controlled by the tumor suppressor p53 (wild type) that upregulates Rnd3 expression in response to DNA damages associated with prolonged metaphase. Rnd3 compartmentalized RhoA activities accumulated during prolonged metaphase to drive cell-in-cell formation. Remarkably, this prolonged mitosis-induced entosis (mintosis) selectively targets non-diploid progenies for internalization, blockade of which increased aneuploidy. Thus, our work uncovered a heretofore unrecognized mechanism of mitotic surveillance for entosis, which eliminates newly-born abnormal daughter cells in a p53-depedent way to maintain genome integrity.

Key Words: mintosis, entosis, mitosis, cell-in-cell, p53, RND3, mitotic surveillance

48 **MAIN TEXT**

49 **Introduction**

50 Cell division via mitosis is strictly regulated to ensure the production of healthy daughter cells.
51 During mitosis, correct segregation and distribution of genetic materials into daughter cells rely on
52 proper activation of spindle assemble checkpoint (SAC) (Musacchio, 2015; Sivakumar & Gorbsky,
53 2015). SAC is activated by unsatisfied microtubule-kinetochore attachment, leading to the
54 recruitment of SAC proteins MAD2, BUBR1 and BUB3 together with CDC20 (Kapanidou *et al*,
55 2017) to kinetochores to form mitotic checkpoint complex (MCC). MCC functions to inhibit
56 anaphase-promoting complex or cyclosome (APC/C), the multisubunit E3 ubiquitin ligase essential
57 for metaphase-anaphase transition in the presence of CDC20. Molecules disrupting MCC such as
58 CUEDC2 could activate APC/C via preventing MAD2 from binding to CDC20 (Gao *et al*, 2011).
59 Activated APC/C promotes proteasome-dependent degradation of cyclin B1 (CCNB1) to allow
60 mitotic exit, and securin to release separase (ESPL1) which leads to cohesion destruction and
61 subsequent sister chromatid separation (Musacchio, 2015; Sivakumar & Gorbsky, 2015). Prolonged
62 SAC activation due to mitotic aberrations generally leads to mitotic arrest and often, but not always,
63 to mitotic catastrophe (specifically referred to catastrophic death here) (Vitale *et al*, 2011). Those
64 that eventually pass mitotic arrest are prone to produce aneuploid/polyploid (non-diploid) daughter
65 cells that need to be dealt with post-mitotically, otherwise impair tissue homeostasis and/or
66 contribute to tumorigenesis (Funk *et al*, 2016; Santaguida & Amon, 2015).

67 Entosis is a recently defined non-apoptotic cell death program, where suspended epithelial cells
68 actively penetrate into and die inside of their neighbors (Overholtzer *et al*, 2007). Cell penetration
69 leads to the formation of so called "cell-in-cell" structures (CIC), which requires polarized
70 actomyosin contraction at the rear cortex of the internalizing cells. The polarized distribution of
71 actomyosin is established by local inhibition of RhoA-ROCK signaling at cell-cell junctions, where
72 lie junction-associated inhibitors, such as p190A RhoGAP (Sun *et al*, 2014a). Multiple factors,

73 including CDKN2A (Liang *et al*, 2018), PCDH7 (Wang *et al*, 2020), IL-8 (Ruan *et al*, 2018a) and
74 membrane cholesterol and lipids (Ruan *et al*, 2018b), that affects RhoA signaling were recently
75 identified as important regulators of entotic CIC formation. Although initially viable, majority of
76 the internalized cells die non-autonomously with the assistance of outer host cells (Florey *et al*,
77 2011). Pathologically in the context of tumors, entosis was proposed as a cellular mechanism of cell
78 competition that selects winner tumor cell clones via internalizing and killing loser cells (Kroemer
79 & Perfettini, 2014; Sun *et al*, 2014b), and promotes tumor evolution by inducing genome instability
80 of outer cells (Krajcovic *et al*, 2011; Mackay *et al*, 2018). However, its roles in physiological context
81 remain largely speculative and mysterious up to date.

82 The tumor suppressor p53 was known as "guardian of genome". In responding to acute DNA
83 damages, signaling cascades involving ATM/ATR and/or CHK1/CHK2 were initiated to activate
84 p53, which was believed to triggers cellular responses such as cell cycle arrest or apoptosis to
85 counteract the genotoxic stresses (Bieging *et al*, 2014). p53 initiates different cellular responses
86 generally via regulating expression of specific downstream target genes, such as the CDK inhibitor
87 *p21* for cell cycle arrest and the pro-apoptotic Bcl-2 family members *Puma* and *Noxa* for apoptosis
88 (Joerger & Fersht, 2016). While cell cycle arrest was envisaged to provide cells an opportunity to
89 fix the repairable DNA damages before next round of cell cycle and thus prevent propagation of
90 potentially harmful mutations, cell death by apoptosis was likely a more aggressive and efficient
91 way to eliminate cells harboring more severe genetic aberrations, and thereby to maintain genome
92 integrity (Bieging *et al.*, 2014; Joerger & Fersht, 2016). In addition to apoptosis, p53 was also
93 implicated in other forms of cell deaths that play roles in removing cells with DNA damages
94 (Kruiswijk *et al*, 2015). Mitotic catastrophe was believed to be a p53-regulated non-apoptotic cell
95 death that eliminates questionable cells during prolonged mitosis which generally takes place with
96 DNA damages (Ranjan & Iwakuma, 2016). Nevertheless, it's unknown whether genetically

97 questionable progenies following mitosis were actively removed by a non-apoptotic cell death that
98 might also be regulated by p53.

99 Here, we demonstrate that p53 mediates the internalization and elimination of aneuploidy
100 daughter cells from transient mitotic arrest by a non-apoptotic death program termed mintosis
101 (derived from prolonged mitosis-induced entosis), which was driven by Rnd3-compartmentalized
102 RhoA activities in daughter cells that were internalized in response to DNA damages during
103 prolonged metaphase. Thus, our work identified a novel surveillance mechanism for entosis, in a
104 wild type p53-depedent way, to safeguard mitosis and genome integrity.

105 **Results**

106 **Entosis is Associated with Prolonged Mitosis**

107 In a process of tracking entotic CIC formation by time lapse microscopy in adherent MCF10A,
108 a non-transformed human mammary epithelial cell line routinely used for entosis research, we
109 unexpectedly found that majority (22/24) of CIC structures formed shortly after mitotic cell division,
110 in spite of a few of exceptions where one adherent cell migrating into and one suspended cells
111 sinking into their neighbors (Figure 1A, C and Movie S1). Once internalized, the inner cells readily
112 underwent cell death (Figure 1B, D, Figure S1 and Movie S2-3) as previously reported for entosis
113 (Overholtzer *et al.*, 2007). The result suggests that mitosis could initiate entosis in adherent
114 monolayers as recently reported for the induced entosis, via CDC42 depletion, in 16HBE cells
115 (Durgan *et al*, 2017). However, only a small portion of the mitotic events (<0.5% or so) led to entosis
116 in normal adherent MCF10A culture, suggesting that entotic mitosis, referring to mitosis leading to
117 entosis, is intrinsically different from normal mitosis. Comparison analysis revealed a significantly
118 prolonged metaphase in entotic mitosis of MCF10A cells (Figure 1A, 1E and Movie S1, 2), Similar
119 entosis also occurred in MCF7, a breast cancer cell line that frequently undergoes entosis (Figure
120 S1C, S1D), indicating that entosis may take place in respond to mitotic arrest.

121 **Transient Mitotic Arrest Activates Entotic CIC Formation**

122 To test this idea, we performed RNAi-mediated knockdown (KD) of CDC20 (Figure 2A) and
123 ESPL1 (Figure S2A), two core genes critical for metaphase to anaphase transition, in MCF10A cells.
124 Both CDC20 and ESPL1 depletion efficiently induced mitotic arrest of various extents (Figure 2B
125 and S2B-C) and importantly increased CIC formation 36 hours post siRNA transfection (Figure 2C
126 and S2D) when a number of mitotically arrested cells started to appear. Similar to that in
127 spontaneous entosis, mitosis is corresponding to majority of CIC formation (47/51 for CDC20 KD,
128 53/54 for ESPL1 KD) for these two induced entosis (Figure 2D and S2E), consistent with which,
129 blocking cell cycle with CDKs' inhibitors (Ro-3306 and SU-9516) efficiently inhibited CIC
130 formation (Figure 2C). Interestingly, while metaphase of normal division peaks around 20 min for
131 MCF10A cells (Figure 2B, 2E and S2C), entotic mitosis displays a restricted metaphase range from
132 30 min to 195 min (Figure 2E and S2C) with most entotic events preceded by mitotic arrest of 60
133 min or so. Mitotic cells arrested for more than 200 min were unlikely capable of division and
134 eventually ended up with catastrophic death (Figure 2E, 2F, S2C and Movie S4). Therefore, mitotic
135 catastrophe and entosis are likely cooperated to safeguard aberrant mitosis with each of them worked
136 before and after mitosis, respectively. To further confirm the role of mitotic arrest in activating
137 entosis, mitotic arrest induced by depleting CUEDC2, a promoter of metaphase-anaphase transition
138 (Gao *et al.*, 2011), was released by co-depleting either BUBR1 or MAD2 (Figure 2G and S2F-H),
139 two essential components of mitotic checkpoint complex (Sivakumar & Gorbsky, 2015). As a result,
140 mitosis-activated CIC formation induced by CUEDC2 depletion was inhibited as well (Figure 2H-
141 I). The impact of mitotic arrest on entosis induction was also confirmed in MCF7 cells (Figure S2I,
142 S2J). Together, the data presented above supports that mitotic arrest, indicated by prolonged
143 metaphase, primes cells to undergo entotic CIC formation post-mitotically. To differentiate from
144 entosis induced via other ways, we refer to this prolonged mitosis-induced entosis as mintosis
145 hereafter.

146 **DNA Damages Promote Mintosis**

147 DNA damages were reported being associated with prolonged mitosis (Ganem & Pellman,
148 2012). We therefore hypothesized that DNA damages might account for mintosis incurred by
149 prolonged mitosis. Consistent with this idea, time lapse-associated immunostaining indicated that
150 cells of longer metaphase were positive in γH2AX (Figure 3A-B, Figure S3A), a marker of DNA
151 damages, with nuclear γH2AX foci significantly more than those in cells of shorter metaphase
152 (Figure 3C). Moreover, the nuclear γH2AX foci were correlated with formation of mintotic CIC
153 structures, where the internalizing mitotic daughter cells contained more nuclear γH2AX foci than
154 their siblings that didn't form CIC structures (Figure 3D). Significantly, mintotic CIC formation
155 was consistently suppressed by γH2AX depletion (Figure 3E-F) or inhibition of its downstream
156 signaling by chemical compounds (Figure 3G) or siRNAs targeting ATM, ATR, CHK1 and CHK2
157 (Figure S3B-C), indicating an essential role of DNA damage signaling in mintosis. To directly
158 examine the effects of DNA damages on mintosis, cells synchronized in M phase were treated with
159 mitomycin, a DNA damage inducer, and then cultured in normal media to allow mitotic exit and
160 cytokinesis. As shown Figure 3H-I, mitomycin treatment efficiently activated DNA damage
161 response, indicated by enhanced expression of γH2AX and phosphorylated ATM (Figure 3H), and
162 significantly increased mintotic CIC formation following cell division (Figure 3I). These effects
163 were confirmed by bleomycin, another DNA damage inducer (data not shown). Interestingly, DNA
164 damage signaling was likely also activated in human breast cancer tissues with high CIC structures,
165 where nuclear γH2AX foci were significantly more than those in low-CIC breast cancer tissues
166 (Figure 3J-K). Together, these data suggest that prolonged mitosis-associated DNA damages induce
167 mintosis.

168 **P53 is Required for Daughter Cells to Undergo Mintosis**

169 Since p53 is the key mediator of DNA damage signaling, we then explore the involvement of
170 p53 in mintosis. Time lapse-associated immunostaining indicated that high level of p53 accumulated

171 in the nuclei of daughter cells penetrating into their neighbors (Figure 4A). The expression levels of
172 p53 were positively correlated with γH2AX foci formation (Figure 4B), and higher in mitotic cells
173 of longer metaphase (Figure 4C), and higher in the internalizing daughter cells as compared with
174 their non-mintotic sibling cells (Figure 4D) and those from normal division (Figure 4E). Importantly,
175 RNA interference-mediated knockdown of p53 significantly suppressed mintotic CIC formation
176 induced by CDC20 or CUEDC2 knockdown (Figure 4F-G), suggesting that p53 is required for
177 mintosis. By a coculture experiment, p53 was demonstrated to function primarily in the mitotic
178 daughter cells that penetrate into their neighbors, as p53 knockdown reduced the frequency of cells'
179 penetration as inners when co-cultured with control cells (Figure 4H-J).

180 **RhoA Activity Accumulated with Prolonged Metaphase Promotes Mintosis**

181 To explore the potential mechanisms underlying the regulation of mintosis by p53, we first
182 examine changes in RhoA activities, which is prerequisite for CIC formation (Ning *et al*, 2015; Sun
183 *et al.*, 2014a) and regulated by p53 signaling (Gadea *et al*, 2007; Xia & Land, 2007), during mintosis.
184 CDC20-depleted cells were stained with antibody for p-MLC, a readout of RhoA activities,
185 following 4-hour time lapse microscopy (Movie S5). As shown in Figure 5A-C, mitotic cells of
186 longer metaphase tended to display higher p-MLC intensity, in agreement with which, RhoA
187 activities in mitotic cells did accumulate over time as monitored by FRET time lapse analysis
188 (Figure 5D, S4A-B and Movie S6). Since mintotic CIC formation occurred in daughter cells, we
189 examined whether enhanced RhoA activities in mother cells could be inherited by daughter cells.
190 RhoA activities of daughter cells right after cytokinesis were compared with those of their respective
191 mother cells in the end of metaphase by FRET time lapse. As shown in Figure S4A-D, the two
192 sibling daughter cells are tightly adherent to their mothers in RhoA activities, which is true for both
193 normal and mintotic cell division, suggesting that RhoA activities could be transmitted from mother
194 cells to daughters with little loss. We then examined the effects of changed RhoA activities on
195 mintotic CIC formation, consistent with essential role of RhoA in entosis, ectopic overexpression

196 of RhoA significantly increased mintotic CIC frequency (Figure 5E), and inhibition of RhoA
197 signaling by Y27632 targeting ROCKs efficiently suppressed mintotic CIC formation (Figure 5F),
198 supporting a role of increased RhoA activity in promoting mintosis.

199 **P53-regulated Rnd3 is Essential for Compartmentalizing RhoA Activities and Mintosis**

200 Since polarized distribution of actomyosin, the downstream effector of RhoA signaling, is
201 essential for cells' penetration into their neighboring cells (Sun *et al.*, 2014a), we examined the
202 expression of p-MLC, the readout of contractile actomyosin and RhoA activity, in the intermediate
203 mintotic CIC structures. As shown in Figure 5G and S4E, p-MLC displays typical asymmetric
204 distribution pattern, characterized by higher intensity at the rear cortex than that at cell-cell junctions
205 marked by E-cadherin where RhoA activities were actively suppressed by inhibitors such as p190A
206 RhoGAP (Sun *et al.*, 2014a). While wild type p53 was known to negatively regulate RhoA signaling
207 through its downstream target Rnd3 (Ongusaha *et al*, 2006; Zhu *et al*, 2014), an atypical Rho
208 GTPase that inhibits RhoA signaling by directly targeting ROCK I (Ongusaha *et al.*, 2006; Riento
209 *et al*, 2003) and p190A RhoGAP (Wennerberg *et al*, 2003). We therefore hypothesized that Rnd3
210 may facilitate CIC formation via helping compartmentalize RhoA activities. In agreement with this
211 notion, Rnd3, regulated by p53 (Figure S4F), specifically localizes at cell-cell junctions while MLC
212 is enriched at the cortical periphery away from junctions during CIC formation (Figure 5H). SiRNA-
213 mediated Knockdown of Rnd3 led to increased pMLC staining at cell-cell junctions (Figure 5I-J
214 and S4G), suggesting that the junctional-localization of Rnd3 spatially restricts RhoA pathway
215 activity and inhibits myosin contraction at cell-cell junctions, which promotes CIC formation.
216 Consequently, Rnd3 depletion significantly inhibited mintotic CIC formation (Figure 5K). Together,
217 the above data fits a model whereby p53-regulated Rnd3 compartmentalizes RhoA activity in
218 daughter cells from prolonged mitosis to drive CIC formation.

219 **Mintosis Selectively Targets Mitotic Progenies of Non-Diploidy**

220 Prolonged metaphase due to SAC activation allows cells to fix problems during chromosome
221 segregation. Nevertheless, prolonged mitosis also elicit structural DNA damages (Dalton *et al*, 2007;
222 Ganem & Pellman, 2012) that, via truncated DNA damage response (DDR), induce whole-
223 chromosome missegregation (Bakhoum *et al*, 2014), leading to non-diploid daughter cells
224 (Bakhoum *et al*, 2017). We therefore hypothesized that mintosis was set to ensure selective
225 elimination of those non-diploid cells. Fluorescent in situ hybridization (FISH) was employed to
226 access ploidy changes in MCF10A cells plated on gridded-glass bottom dish following 24 hour-
227 time lapse microscopy, and the metaphase and position histories of target cells were determined by
228 retroactive review of the time lapse records (Movie S7). While mitosis of short metaphase, based
229 on the probes used, generally gave rise to diploid progenies (96.9%) (Figure 6A and 6C), cells of
230 prolonged metaphase penetrating their neighbors to form CIC structures were largely non-diploid
231 (50.7%) (Figure 6B, 6D and S5A). This non-diploid rate of mintotic inner cells is similar to that
232 (43.9%) of inner cells of pre-existing CIC structures (Figure 6E), consistent with our observation
233 that majority of CIC structures were from prolonged mitosis. Intriguingly, the sibling cells that did
234 not participate into CIC formation were largely diploid (88.5%) (Figure 6F) in a rate similar to the
235 whole MCF10A population (89.9%) (Figure 6G). And a small portion of inner cells that eventually
236 got released from CIC structures were also largely diploid (83.8%) (Figure 6H and Figure S5B).
237 Therefore, mintosis selectively targets non-diploid daughter cells for elimination, which may play
238 an essential role in maintaining population genetic integrity, as blocking mintosis by Y27632, an
239 inhibitor of ROCK kinases prerequisite for CIC formation (Sun *et al.*, 2014b), significantly
240 increased non-diploid cells in the cell population (Figure 6I). Thus, our data support that p53-
241 regulated mintosis may serve as a cellular mechanism of mitotic surveillance.

242 **Discussion**

243 In summary, we proposed a CIC-mediated mechanism of post-mitotic surveillance as mintosis
244 whereby non-diploid progenies from prolonged mitosis were eliminated in a p53-dependent manner.

245 In this model (Figure 7), γH2AX-marked DNA damages associated with prolonged mitosis in
246 mother cells activate p53 pathway in daughter cells that are non-diploid due to chromosome
247 missegregation, p53 upregulates the expression of its downstream target Rnd3 which locally inhibits
248 RhoA signaling and actomyosin contraction at cell-cell junctions, leading to asymmetric RhoA
249 activation at the rear cortex of daughter cells to drive cell internalization and subsequent non-
250 apoptotic death. Thus, this work uncovered a novel non-apoptotic mechanism by mintosis for p53
251 to maintain genome integrity.

252 DNA damages associated with mitosis are generally phenotyped as prolonged mitosis or mitotic
253 arrest, which could also cause DNA damages (Dalton *et al.*, 2007; Ganem & Pellman, 2012).
254 Formation of this vicious loop is largely due to impaired DNA damage response (DDR) which,
255 though being capable of sensing DNA damages, likely stops short of downstream damage repair
256 pathways (Heijink *et al*, 2013). Though activation of this partial DDR was believed to prevent fusion
257 of exposed telomeres under normal circumstance (Orthwein *et al*, 2014), it left unrepaired DNA
258 damages, pre-mitotic or acquired, into mitotic progenies under stressed conditions (Denchi & Li,
259 2014). Moreover, activation of the partial DDR during mitosis, instead helps fix errors in DNA,
260 actually could result in severe chromosome missegregation, which eventually gives rise to aneuploid
261 progenies (Bakhoum *et al.*, 2017; Bakhoum *et al.*, 2014). Therefore, surveillance mechanisms are
262 critical to deal with daughter cells from prolonged mitosis. Previous studies indicated that prolonged
263 mitotic progenies might be surveilled by either growth arrest or apoptosis (Joerger & Fersht, 2016;
264 Lambrus & Holland, 2017; Vitale *et al.*, 2011). Whereas in this study, we identified a novel
265 surveillance mechanism executed by CIC-mediated non-apoptotic death termed mintosis. Although
266 aslo being activated by prolonged mitosis via p53-dependent pathway, mintosis likely represents a
267 unique process independent from growth arrest and apoptosis because depleting p21, a p53 downstream
268 effector that is required for growth arrest/senescence, didn't block mintotic CIC formation at all (data
269 not shown), and depletion of Rnd3, a p53 target gene that was identified as suppressor of ROCK I-

270 mediated apoptosis (Ongusaha *et al.*, 2006; Paysan *et al*, 2016), significantly suppress mintosis
271 (Figure 5I-K).

272 Interestingly, while our work demonstrates a positive role of CIC formation in maintaining
273 genome stability by eliminating aneuploidy cells, previous work supported entosis as a cellular
274 mechanism to promote genome instability by inducing aneuploidy (Krajcovic *et al.*, 2011). This
275 clear conceptual discrepancy is actually due to different cellular and molecular contexts where CIC
276 formation may work. At cellular level, Krajcovic *et al* found that the presence of inner cell could
277 physically block cytokinesis of outer cell, leading to outer cell binucleation and subsequent
278 aneuploidy of its offspring following next round of cell division (Krajcovic *et al.*, 2011). This effect
279 may be propagated to promote genome instability in the context of tumor cells that are tolerated to
280 aneuploidy. This idea was supported by recent work in lung cancer cells Mackay *et al* (Mackay *et*
281 *al.*, 2018). Whereas this work investigates CIC's role in a non-tumor context, in which aneuploid
282 daughters from prolonged mitosis were internalized as inner cells and eliminated. Thus, it's likely
283 that CIC formation affects genome stability differentially via inner cell and outer cell, respectively,
284 depending on cells' tolerance to aneuploidy. For tumor cells who are generally aneuploidy-tolerant,
285 CIC formation may promote genome instability by inducing cytokinesis failure of outer cells; for
286 non-transformed epithelial cells, CIC formation may function to counteract genome instability by
287 internalizing and eliminating aneuploid cells. Of note, since aneuploidy is toxic and lethal to non-
288 transformed cells, the aneuploid progenies of binucleated outer cells wouldn't survive for long
289 period (data not shown). This is also true for tumor cells that are not tolerant to aneuploidy (Mackay
290 *et al.*, 2018). Therefore, CIC formation is genome instability- or tumor-suppressive anyway when
291 cells are not tolerant to aneuploidy. At molecular level, CIC's effects on aneuploidy and genome
292 stability are controlled by p53 status. Mackay *et al* found that only mutant p53, but not wild type or
293 null p53, could promote genome instability via CIC formation by conferring cancer cells
294 winner/outer identity and allowing survival and population of their aneuploidy progenies (Mackay

295 *et al.*, 2018). Whereas, our work demonstrated that wild type p53 endowed loser/inner identity to
296 cells during CIC formation by facilitating the establishment of polarized RhoA activities. Together,
297 we propose that CIC formation, depending on p53 status, may play dual roles in genome instability
298 and tumorigenesis as well. For cancer cells with mutant p53, CIC formation plays promotive role
299 by facilitating selection of cancer cells harboring mutant p53; for normal epithelial cells or cancer
300 cells that contain wild type p53, CIC formation play suppressive role by eliminating aneuploidy
301 cells expressing wild type p53 through mintosis. It'll be of interest to explore whether other
302 oncogenic mutations may also regulate CIC's functional outcomes.

303 Recently, two other works reported entosis induction in confined contexts in adherent
304 monolayer cultures (Durgan *et al.*, 2017; Hamann *et al*, 2017). One of work demonstrated that
305 glucose starvation, an extreme biological condition, was capable of promoting CIC formation
306 mainly in the context of cancer cells like MCF7 in an AMP activated protein kinase (AMPK)-
307 dependent way (Hamann *et al.*, 2017). Interestingly, although AMPK is a well-known energy sensor,
308 it was found in mitotic apparatus and involved in the regulation of mitotic progression and
309 completion (Banko *et al*, 2011; Li & Zhang, 2017). So we hypothesize that glucose induced
310 activation of AMPK may influence normal mitosis, which triggers mintosis and contributes to CIC
311 formation in adherent cells that is yet to be validated. Another work reported that depletion of
312 CDC42, a polarity protein, induced CIC formation in 16HBE cells (Durgan *et al.*, 2017). Although
313 mitosis was found linked to CIC formation, the work failed to identify the essential role of mitotic
314 arrest and DNA damages in CIC formation, hence, couldn't tell why most mitosis failed to give rise
315 to CIC structures and why reagents blocking mitosis unexpectedly induced CIC formation.
316 Intriguingly, similar to work by Wan et al (Wan *et al*, 2012), where depletion of polarity protein
317 PAR3 resulted in enhanced formation of CIC structures in adherent MDCK cells, polarity changes
318 were not regarded as the reason for enhanced CIC formation (Durgan *et al.*, 2017; Wan *et al.*, 2012).
319 Whereas, we found that depleting polarity protein such as CDC42 in MCF10A and tumor cells could

320 promote CIC formation that was also preceded by prolonged mitosis (data not shown), we therefore
321 speculate that altered mitosis might be a shared route for multiple factors, such as glucose starvation
322 and depleting polarity proteins and the like, to activate mintosis that works in multiple contexts to
323 maintain homeostasis.

324

325 **Materials and Methods:**

326 **Cell culture and constructs.** MCF7 and 293FT cells were maintained in Dulbecco's modified
327 Eagle's medium (DMEM) supplemented with 10% fetal bovine serum (PAN-Biotech). MCF10A
328 and its derivatives were cultured in DMEM/F12 supplemented with 5% horse serum (GIBCO,
329 #16050-122), 20 ng/ml EGF (Peprotech, #96-AF-100-15-100), 10 µg/ml insulin (Sigma, I-5500),
330 0.5 µg/ml hydrocortisone (Macgene, CC103), and 100 ng/ml cholera toxin (Sigma, C8052). pBabe-
331 H2B-mCherry was a gift from Dr. Michael Overholtzer. pBabe-RhoA biosensor was a gift of Dr.
332 Klaus Hahn from Addgene (12602). pLKO-shp53 was a gift of Dr. Bob Weinberg from Addgene
333 (19119). GFP-p53 was a gift of Dr. Tyler Jacks from Addgene (12091). Expression plasmid for
334 GFP-Rnd3 was constructed by inserting synthesized human Rnd3 ORF into pQCXIP-GFP vector
335 by *Xho* I and *Bam*H I sties. Expression plasmid for MLC-mCherry was constructed by inserting
336 synthesized chicken MLC ORF into pBabe-mCherry vector by *Xho* I and *Bam*H I sties.

337 **Antibodies and chemical reagents.** Antibodies with working dilution factors, company source and
338 catalog number include: anti-pMLC (1:200; Cell Signaling; #3671), anti-E-cadherin (1:200; BD
339 Biosciences; 610181), anti-γH2AX (1:200; Cell Signaling; #9718 for IF; 1:500; ABclonal; AP0099
340 for WB), anti-H2AX (1:1000; ABclonal; AP0823), anti-pATM (1:500; Boster; BM4008), anti-
341 ATM (1:1000; Proteintech; 27156-1-AP), anti-pp53 (1:500; Cell Signaling; #9386), anti-p53
342 (1:1000; Santa Cruz; sc-126), anti-Rnd3 (1:1000; Sino Biological; 101056-T32). Secondary
343 antibodies include Alexa Fluor 568 anti-mouse (1:500; Invitrogen; A11031), Alexa Fluor 568 anti-
344 rabbit (1:500; Invitrogen; A11036), Alexa Fluor 488 anti-mouse (1:500; Invitrogen; A11029) and
345 Alexa Fluor 488 anti-rabbit (1:500; Invitrogen; A11034). Alexa Fluor®647 Phalloidin (1:200;
346 Invitrogen; A22287). DAPI was purchased from Sigma (D8417). ROCK inhibitor Y27632 was
347 purchased from TOCRIS (1254) and used at final concentration of 10 µM. Ro-3306 (HY-12529), a
348 potent and selective inhibitor of CDK1, and SU-9516 (HY-18629), a selective CDK2 inhibitor, were
349 purchased from MedChem Express. DNA damage inducers Mitomycin (T6890) and Bleomycin

350 (T6116), and inhibitors for ATM (T2474), ATR (T3338), CHK1 (T2033), CHK2 (T7080) were
351 purchased from TargetMol. Collagen Type I is a product of BD Biosciences (#354236).

352 **Virus production and infection.** Stable expression cell lines were established by virus infection.
353 Briefly, $1x10^6$ 293FT cells were plated into 6-well plate coated with collagen I (BD Bioscience,
354 #354236), transfection was performed with retroviral constructs together with packaging plasmids,
355 and viruses were collected twice at 24 h intervals. To infect cells, cells were cultured in 1 ml viral
356 supernatant mixed with 1 µl polybrene of 10 µg/ml stock for 6 h followed with regular media. Cells
357 were selected with appropriate antibiotics (2 µg/ml puromycin or 400 µg/ml G418 for MCF10A,
358 1µg/ml puromycin for MCF7) for 7 days.

359 **RNA interference.** siRNAs were from GenPharma (Shanghai, China). For individual siRNA trans
360 fection, cells ($1x10^5$/well) were plated into 12-well glass bottom plate and cultured overnight, then
361 transfected with 50 nM siRNA using Lipofectamine® RNAiMAX (Invitrogen, #13778-150). Cell
362 s were fed with fresh full media 6 h later. siRNA sequences: CUEDC2: 5'-CAUCAGAGGAGAA
363 CUUCGA-3'; CDC20: 5'-CCACCAUGAUGUUCGGGUATT-3'; MAD2 : 5'-GGAAGAGUCGG
364 GACCACAGTT-3'; BuBR1: 5'-CGGGCAUUUGAAUAUGAAATT-3'; ESPL1: 5'-GCUUGUGA
365 UGCCAUCCUGATT-3'; H2AX-1: 5'- GGGACGAAGCACUUGGUAACA-3'; p53-1: 5'- AAGA
366 CUCCAGUGGUAAUCUAC-3'; Rnd3-1: 5'- GAUCCUAAUCAGAACGUGAAA-3'; Rnd3-2: 5'-
367 AUCCUAAUCAGAACGUGAAAU-3'; ATM: 5'- GCCUCCAAUUCUUCACAGUAA-3'; ATR:
368 5'- GAUGAACACAUGGGAUAUUUA-3'; CHK1-1: 5'- GUGACAGCUGUCAGGAGUAUU-3';
369 CHK1-2: 5'- GCCCACAUGUCCUGAUCAUAU-3'; CHK2-1: 5'- GAACAGAUAAAUACCGAA
370 CAU-3'; CHK2-2: 5'- CGCCGUCCUUUGAAUAACAAU-3'; Negative Control: 5'-UCUCCGAA
371 CGUGUCACGUTT-3'.

372 **Reverse transcription-quantitative PCR (RT-qPCR).** Total RNA was isolated from cells 48 h a
373 fter siRNA transfection using TRIzol reagent (Invitrogen, #15596026). One microgram of total RN
374 A was converted into cDNA using *TransScript*® One-Step gDNA Removal and cDNA Synthesis S

375 uperMix (Transgen Biotech, #AT311-02) according to manufacturer's instruction. The quantitativ
376 e PCR (qPCR) was performed on 15 ng of cDNA from each sample using SYBR Green Real-time
377 PCR Master Mix (TOYOBO, #QPK-201) based on the recommendations of manufacturer. Primers
378 pairs spanning at least two exons were confirmed by NCBI Primer-BLAST: CUEDC2: 5'-TGAG
379 CGATGCCAGGAACAA-3' and 5'-CTCCTCCTCAGCGCCAGTT-3'; CDC20: 5'-TTCCCTGCC
380 AGACCGTATCC-3' and 5'-CAGCCAAGTAGTTGCCCTC-3'; MAD2: 5'-TTCTCATTCGGCAT
381 CAACA-3' and 5'-TCTTTCCAGGACCTCACCA-3'; BuBR1: 5'-TCTTCAGCAGCAGAAACGG
382 -3' and 5'-TCATTGCATAAACGCCCTA-3'; ESPL1: 5'-CCCCACTTCGGGCATTGTA-3' and 5'-
383 GGGCAAAGTCATAAACCACC-3'; BUB1: 5'-AGAAATACCACAATGACCCAA-3' and 5'-AG
384 GCGTGTCTGAAATAACC-3'; H2AX: 5'- CCCTTCCAGCAAACTCAACTCG-3' and 5'- AAAC
385 TCCCCAATGCCTAAGGT-3'; p53: 5'- ACCACCATCCACTACAACTACAT-3' and 5'- CTCCC
386 AGGACAGGCACAAA-3'; Rnd3: 5'- TCTTACCCTGATTCGGATGC-3' and 5'- TCTGACGCTA
387 TTTTCCGACT-3'; ATM: 5'- GCACAGAAGTGCCTCCAATTC-3' and 5'- ACATTCTGGCACG
388 CTTTG-3'; ATR: 5'- GCCGTTCTCCAGGAATACAG-3' and 5'- GAGCAACCGAGCTTGAGAG
389 T-3'; CHK1: 5'- GGATGCGGACAAATCTTACCA-3' and 5'- CCTTAGAAAGTCGGAAGTCAA
390 CC-3'; CHK2: 5'- GTCATCTCAAGAAGAGGACT-3' and 5'- GAGCTGTGGATTCATTTTCC-3
391 '; HPRT: 5'-AGGCCATCACATTGTAGCCCTCTGT-3' and 5'-TACTGCCTGACCAAGGAAAG
392 CAAAGT-3'. The PCR reactions run on the following conditions: initial denaturing at 95°C for 30
393 sec, followed by 35–40 cycles of 95°C for 5 sec, 60°C for 10 sec and 72°C for 15 sec, melting cur
394 ves were examined at 37°C for 30 sec before cooling. Each result was from three independent biol
395 ogical replicates for all analyses performed in this work. The qPCR results were analyzed using $2^{-\Delta}$
396 $^{\Delta C_T}$ method and presented as relative quantity of transcripts with HPRT as the reference gene.

397 **Cytospin and entotic CIC quantification.** Described protocol (Sun & Overholtzer, 2013) was
398 slightly modified to examine cells abilities to form CIC structures. Briefly, cells were cultured in
399 suspension for 6 h in 6-well plate pre-coated with 1 ml solidified soft agar (0.5%) and then mounted

400 onto glass slides for 3-min centrifugation at 400 rpm to make cytospin. Cells were fixed by 4% PFA
401 and immunostained with E-cadherin antibodies followed by mounting with Antifade reagent with
402 DAPI. CIC structures with more than half of cell body internalized were counted.

403 **Time lapse imaging and mintotic CIC quantification.** Wide field imaging was performed on cells
404 plated in glass bottom dish or plate (Nest Biotechnology Co.) by Nikon Ti-E microscope equipped
405 with motorized stage and Neo Vacuum cooled Scientific CMOS Camera (Andor Technology).
406 Images were collected every 10 or 15 min for 24 h using 10x or 20x Apo objective lens with 15 ms
407 exposure for DIC channel and 150 ms exposure for mCherry channel. Cells were cultured in
408 humidified chamber supplied with 5% CO_2 at 37°C during imaging. Image sequences were reviewed
409 using Nikon NIS-Elements AR 4.5 software. Mitotic entry was judged morphologically by either
410 condensed chromatin as indicated by H2B-mCherry condensation or cells' round up. Mitotic
411 anaphase was judged by chromosome separation labeled with H2B-mCherry. The duration of
412 metaphase was determined from the first frame of mitotic entry to the first frame of mitotic anaphase.
413 CIC structures were determined morphologically by complete enwrapping of cells into their
414 neighbors, typically with a crescent nucleus in the outer cells. Total cells in each field were counted
415 on mCherry-postive nuclei. CIC frequency was presented as CIC number divided by total cells in
416 each field.

417 For CIC formation induced by DNA damages, MCF10A/H2B-mCherry cells in 12 well plate
418 (2.5*10^4/well) were synchronized by 100ng/m nocoldazole for 6 h followed by treatment of DNA
419 damage inducers mitomycin (0.5 μM, 1 μM, 2 μM) for 3.5 h. Then, drugs were washed out for 20
420 h time lapse in full medium. CIC formation was quantified as did above.

421 **Time lapse-associated FISH (fluorescence in situ hybridization).** Prior to FISH, MCF10A cells
422 of 3×10^5 were first cultured in gridded glass bottom dish (μ-Dish 35mm Grid-500, ibidi; #81168)
423 for 20 h, followed by time lapse microscopy with images collected every 10 min for 16 h by using
424 10x Apo objective lens in DIC channel. Then, cells were immediately fixed at room temperature for

425 20 min with freshly prepared solution (methanol/glacial acetic acid = 3:1) after briefly washed twice
426 with PBS. Fixed cells were initially baked at 56 °C for 60 min, subsequently incubated in 100 μg/ml
427 RNase (pH=7.0±0.2) for 1 h and then 20 mg/ml pepsin-0.01 M HCl for 10 min at 37 °C. After
428 washed twice with 2× SSC at room temperature for 5 min, samples were dehydrated in 70%, 85%,
429 and 100% pre-cooled ethanol for 2 min respectively, and then air-dried. Hybridization was
430 performed with two-probe FISH kit (F01010-00, GP Medical Technologies, Ltd) following the
431 manual provided. Briefly, sample was denatured at 75°C for 10 min and then preceded to
432 hybridization at 42°C for 16 h in a humidified cassette. Following hybridization, sample was serially
433 washed with 0.4x SSC containing 0.3% NP-40 (pH=7.0±0.2) at 65 °C for 3 min, 2x SSC containing
434 0.1% NP-40 (pH=7.0±0.2) at room temperature for 1 min and finally 70% ethanol at room
435 temperature for 3 min before counterstained with DAPI in darkness for 10-15 min and mounted.
436 Images were taken by using *Ultraview Vox* spinning disc confocal system (Perkin Elmer) equipped
437 with a Yokogawa CSU-X1 spinning disc head and EMCCD camera (Hamamatsu C9100-13) on
438 Nikon Ti-E microscope. Analysis was performed with Volocity software (Perkin Elmer).
439 Information on cell position, division and CIC formation were determined based on time lapse
440 imaging and grids on the glass bottom.

441 **Time lapse-associated immunostaining (TLAS).** For phospho-Myosin Light Chain 2 (pMLC)
442 staining in mitotic cells, MCF10A/H2B-mcherry cells in gridded glass bottom dish (μ-Dish 35mm
443 Grid-500) were transfected with CDC20 siRNA as described above. Time lapse imaging was
444 performed by 10x Apo objective lens in DIC and mCherry channels next day, with images captured
445 every 10 min for 4 h before fixing with 4% PFA and preceded to routine staining. Briefly, the fixed
446 sample was permeabilized with 0.2% Triton-X 100/PBS for 5 min and blocked with 5% BSA for 1
447 h before incubated with primary antibody at 4°C overnight followed fluorophore-labeled secondary
448 antibody, cells were then co-stained with phalloidin and DAPI for 20 min and then mounted with
449 Prolong Gold antifade reagent (Invitrogen). Images were captured with Nikon Ti-E microscope

450 equipped with Neo Vacuum cooled Scientific CMOS Camera (Andor Technology) and analyzed
451 with Nikon NIS-Elements AR 4.5 software. Mean pMLC intensity of individual cell was calculated
452 by equation: (pMLC-background)/area. TLAS of γH2AX and p53 were performed following the
453 protocol for pMLC with slight modification that time lapse was performed for 20 h in control or
454 CUEDC2-depleted MCF10A cells.

455 **Immunostaining and Immunoblotting**. Cultured cells were stained following protocol above in
456 TLAS. For tissue sections, samples were first deparaffinized and antigen retrieved following routine
457 procedures and then preceded to immunostaining as did in fixed cells above. Confocal images were
458 captured and processed by *Ultraview Vox* confocal system (Perkin Elmer) on Nikon Ti-E
459 microscope. Immunoblotting was performed following standard precedures, briefly, protein
460 samples were separated by SDS-PAGE and then transferred onto PVDF membrane, where specific
461 antibodies were used to probe target proteins.

462 **FRET.** Briefly, activation levels of RhoA were measured by monitoring the ratio of ECFP to
463 Citrine-YFP FRET and ECFP intensities (Pertz *et al*, 2006; Sun *et al.*, 2014a). Images were acquired
464 on a Nikon Ti-E inverted microscope using a Neo Vacuum cooled Scientific CMOS Camera (Andor
465 Technology) mounted on the bottom port with a set of excitation/emission filter wheels to direct the
466 DIC, ECFP, FRET, and Citrine-YFP signals sequentially. Images were obtained using a Nikon
467 20x/0.75 CFI Plan Apochromat Lambda lens and Nikon NIS-Elements AR 4.5 software. The filter
468 sets used for ratiometric imaging were (Excitation, emission, respectively, Chroma Technology):
469 ECFP: ET438/24, ET482/35; FRET: ET438/24, ET540/30; and Citrine-YFP: ET513/17, ET540/30.
470 Cells were illuminated by LUMENCOR SPECTRA X Light Engine with 438/24 and 513/17
471 excitation filters. CFP, FRET and DIC images were recorded with 1 x 1 binning. The FRET module
472 of Nikon NIS-Elements AR 4.5 software was used to process image sequences. The background-
473 subtracted images from two cameras were aligned to ascertain optimal registration with subpixel
474 accuracy. A linear rainbow pseudocolor lookup table was applied to the ratiometric images.

475 **Patient samples.** Breast cancer sections were obtained from 307 Hospital under the hospital's
476 regulations and ethics. Sections stained with E-cadherin or HER2 were scanned by NanoZoomer-
477 SQ (Hamamatsu) digital slide scanning system. CIC structures were judged by fully enclosing of
478 one or more cells within another cell based on membrane contour line. Patient sections were first
479 screened based on the number of CIC structures in fields of 40x magnification, those that had less
480 than 1 CIC structures in more than 3 fields were scored as low CIC, more than 15 CIC structures in
481 3 fields as high CIC.

482 **Statistics.** All assays were carried out in triplicate or more. Data were expressed as means with
483 standard deviations (SD) or standard error of mean (SEM). *P*-values were calculated using two-
484 tailed Student's t-test from Excel or GraphPad Prism software, and *P*-values less than 0.05 were
485 considered statistically significant. Logistic regression analysis in Excel was used to evaluate
486 association between factors.

487

488 **H2: Supplementary Materials**

489 Figure S1. Entosis is coupled with mitotic cell division.

490 Figure S2. Prolonged mitosis primes cells to undergo entosis.

491 Figure S3. Involvement of DNA damage pathway in mintosis.

492 Figure S4. Compartmentalized RhoA activity by Rnd3 is required for mintosis.

493 Figure S5. Mintosis selectively targets non-diploid cells for elimination.

494 Movie S1. The formation of entotic CIC structures.

495 Movie S2. Entosis is coupled with mitotic cell division.

496 Movie S3. Inner cell fates in CIC structures.

497 Movie S4. Catastrophic cell death of mitosis.

498 Movie S5. Mitosis of different metaphase.

499 Movie S6. RhoA activity by FRET during one-cell mintosis.

500 Movie S7. Time lapse for FISH.

501

502

503 **References and Notes**

504 Bakhoum SF, Kabeche L, Compton DA, Powell SN, Bastians H (2017) Mitotic DNA Damage Response: At the
505 Crossroads of Structural and Numerical Cancer Chromosome Instabilities. *Trends in cancer* 3: 225-234
506 Bakhoum SF, Kabeche L, Murnane JP, Zaki BI, Compton DA (2014) DNA-damage response during mitosis induces
507 whole-chromosome missegregation. *Cancer discovery* 4: 1281-1289
508 Banko MR, Allen JJ, Schaffer BE, Wilker EW, Tsou P, White JL, Villen J, Wang B, Kim SR, Sakamoto K *et al*
509 (2011) Chemical genetic screen for AMPKalpha2 substrates uncovers a network of proteins involved in mitosis.
510 *Molecular cell* 44: 878-892
511 Bieging KT, Mello SS, Attardi LD (2014) Unravelling mechanisms of p53-mediated tumour suppression. *Nature*
512 *reviews Cancer* 14: 359-370
513 Dalton WB, Nandan MO, Moore RT, Yang VW (2007) Human Cancer Cells Commonly Acquire DNA Damage
514 during Mitotic Arrest. *Cancer research* 67: 11487-11492
515 Denchi EL, Li J (2014) Let it go: how to deal with a breakup in mitosis. *Nature structural & molecular biology* 21:
516 433-435
517 Durgan J, Tseng YY, Hamann JC, Domart MC, Collinson L, Hall A, Overholtzer M, Florey O (2017) Mitosis can
518 drive cell cannibalism through entosis. *eLife* 6: 1-26
519 Florey O, Kim SE, Sandoval CP, Haynes CM, Overholtzer M (2011) Autophagy machinery mediates macroendocytic
520 processing and entotic cell death by targeting single membranes. *Nat Cell Biol* 13: 1335-1343
521 Funk LC, Zasadil LM, Weaver BA (2016) Living in CIN: Mitotic Infidelity and Its Consequences for Tumor
522 Promotion and Suppression. *Developmental cell* 39: 638-652
523 Gadea G, de Toledo M, Anguille C, Roux P (2007) Loss of p53 promotes RhoA-ROCK-dependent cell migration and
524 invasion in 3D matrices. *The Journal of cell biology* 178: 23-30
525 Ganem NJ, Pellman D (2012) Linking abnormal mitosis to the acquisition of DNA damage. *The Journal of cell*
526 *biology* 199: 871-881
527 Gao YF, Li T, Chang Y, Wang YB, Zhang WN, Li WH, He K, Mu R, Zhen C, Man JH *et al* (2011) Cdk1-
528 phosphorylated CUEDC2 promotes spindle checkpoint inactivation and chromosomal instability. *Nature cell biology*
529 13: 924-933
530 Hamann JC, Surcel A, Chen R, Teragawa C, Albeck JG, Robinson DN, Overholtzer M (2017) Entosis Is Induced by
531 Glucose Starvation. *Cell Rep* 20: 201-210
532 Heijink AM, Krajewska M, van Vugt MA (2013) The DNA damage response during mitosis. *Mutation research* 750:
533 45-55
534 Joerger AC, Fersht AR (2016) The p53 Pathway: Origins, Inactivation in Cancer, and Emerging Therapeutic
535 Approaches. *Annual review of biochemistry* 85: 375-404
536 Kapanidou M, Curtis NL, Bolanos-Garcia VM (2017) Cdc20: At the Crossroads between Chromosome Segregation
537 and Mitotic Exit. *Trends Biochem Sci* 42: 193-205
538 Krajcovic M, Johnson NB, Sun Q, Normand G, Hoover N, Yao E, Richardson AL, King RW, Cibas ES, Schnitt SJ *et*
539 *al* (2011) A non-genetic route to aneuploidy in human cancers. *Nat Cell Biol* 13: 324-330
540 Kroemer G, Perfettini J-L (2014) Entosis, a key player in cancer cell competition. *Cell Res* 24: 1280-1281
541 Kruiswijk F, Labuschagne CF, Vousden KH (2015) p53 in survival, death and metabolic health: a lifeguard with a
542 licence to kill. *Nature reviews Molecular cell biology* 16: 393-405
543 Lambrus BG, Holland AJ (2017) A New Mode of Mitotic Surveillance. *Trends in cell biology* 27: 314-321
544 Li Z, Zhang X (2017) Kinases Involved in Both Autophagy and Mitosis. *International journal of molecular sciences*
545 18
546 Liang J, Fan J, Wang M, Niu Z, Zhang Z, Yuan L, Tai Y, Chen Z, Song S, Wang X *et al* (2018) CDKN2A inhibits
547 formation of homotypic cell-in-cell structures. *Oncogenesis* 7: 1-8
548 Mackay HL, Moore D, Hall C, Birkbak NJ, Jamal-Hanjani M, Karim SA, Phatak VM, Pinon L, Morton JP, Swanton
549 C *et al* (2018) Genomic instability in mutant p53 cancer cells upon entotic engulfment. *Nat Commun* 9: 3070
550 Musacchio A (2015) The Molecular Biology of Spindle Assembly Checkpoint Signaling Dynamics. *Current biology :*
551 *CB* 25: R1002-1018
552 Ning X, Luo T, Chen Z, Sun Q (2015) The physics for the formation of cell-in-cell structures. *Current molecular*
553 *medicine* 15: 867-872
554 Ongusaha PP, Kim HG, Boswell SA, Ridley AJ, Der CJ, Dotto GP, Kim YB, Aaronson SA, Lee SW (2006) RhoE is a
555 pro-survival p53 target gene that inhibits ROCK I-mediated apoptosis in response to genotoxic stress. *Current*
556 *biology : CB* 16: 2466-2472
557 Orthwein A, Fradet-Turcotte A, Noordermeer SM, Canny MD, Brun CM, Strecker J, Escribano-Diaz C, Durocher D
558 (2014) Mitosis inhibits DNA double-strand break repair to guard against telomere fusions. *Science* 344: 189-193
559 Overholtzer M, Mailleux AA, Mouneimne G, Normand G, Schnitt SJ, King RW, Cibas ES, Brugge JS (2007) A
560 nonapoptotic cell death process, entosis, that occurs by cell-in-cell invasion. *Cell* 131: 966-979

561 Paysan L, Piquet L, Saltel F, Moreau V (2016) Rnd3 in Cancer: A Review of the Evidence for Tumor Promoter or
562 Suppressor. *Molecular cancer research : MCR* 14: 1033-1044
563 Pertz O, Hodgson L, Klemke RL, Hahn KM (2006) Spatiotemporal dynamics of RhoA activity in migrating cells.
564 *Nature* 440: 1069-1072
565 Ranjan A, Iwakuma T (2016) Non-Canonical Cell Death Induced by p53. *International journal of molecular sciences*
566 17
567 Riento K, Guasch RM, Garg R, Jin B, Ridley AJ (2003) RhoE binds to ROCK I and inhibits downstream signaling.
568 *Molecular and cellular biology* 23: 4219-4229
569 Ruan B, Wang C, Chen A, Liang J, Niu Z, Zheng Y, Fan J, Gao L, Huang H, Wang X *et al* (2018a) Expression
570 profiling identified IL-8 as a regulator of homotypic cell-in-cell formation. *BMB Rep* 51: 412-417
571 Ruan B, Zhang B, Chen A, Yuan L, Liang J, Wang M, Zhang Z, Fan J, Yu X, Zhang X *et al* (2018b) Cholesterol
572 inhibits entotic cell-in-cell formation and actomyosin contraction. *Biochem Biophys Res Commun* 495: 1440-1446
573 Santaguida S, Amon A (2015) Short- and long-term effects of chromosome mis-segregation and aneuploidy. *Nature*
574 *reviews Molecular cell biology* 16: 473-485
575 Sivakumar S, Gorbsky GJ (2015) Spatiotemporal regulation of the anaphase-promoting complex in mitosis. *Nature*
576 *reviews Molecular cell biology* 16: 82-94
577 Sun Q, Cibas ES, Huang H, Hodgson L, Overholtzer M (2014a) Induction of entosis by epithelial cadherin
578 expression. *Cell Res* 24: 1288-1298
579 Sun Q, Luo T, Ren Y, Florey O, Shirasawa S, Sasazuki T, Robinson DN, Overholtzer M (2014b) Competition
580 between human cells by entosis. *Cell Res* 24: 1299-1310
581 Sun Q, Overholtzer M (2013) Methods for the Study of Entosis. In: *Methods in Mol Biol-Necrosis*, McCall K., Klein
582 C. (eds.) pp. 59-66. Humana Press:
583 Vitale I, Galluzzi L, Castedo M, Kroemer G (2011) Mitotic catastrophe: a mechanism for avoiding genomic
584 instability. *Nature reviews Molecular cell biology* 12: 385-392
585 Wan Q, Liu J, Zheng Z, Zhu H, Chu X, Dong Z, Huang S, Du Q (2012) Regulation of myosin activation during cell-
586 cell contact formation by Par3-Lgl antagonism: entosis without matrix detachment. *Mol Biol Cell* 23: 2076-2091
587 Wang C, Chen A, Ruan B, Niu Z, Su Y, Qin H, Zheng Y, Zhang B, Gao L, Huang H *et al* (2020) PCDH7 Inhibits the
588 Formation of Homotypic Cell-in-Cell Structure *Frontiers in cell and developmental biology*
589 Wennerberg K, Forget MA, Ellerbroek SM, Arthur WT, Burridge K, Settleman J, Der CJ, Hansen SH (2003) Rnd
590 proteins function as RhoA antagonists by activating p190 RhoGAP. *Current biology : CB* 13: 1106-1115
591 Xia M, Land H (2007) Tumor suppressor p53 restricts Ras stimulation of RhoA and cancer cell motility. *Nature*
592 *structural & molecular biology* 14: 215-223
593 Zhu Y, Zhou J, Xia H, Chen X, Qiu M, Huang J, Liu S, Tang Q, Lang N, Liu Z *et al* (2014) The Rho GTPase RhoE is
594 a p53-regulated candidate tumor suppressor in cancer cells. *International journal of oncology* 44: 896-904
595

596 **Acknowledgments**

597 We thank Dr. Overholtzer from Memorial Sloan-Kettering Cancer Center for providing cell lines
598 and reagents. We thank Dr. Louis Hodgson from Albert Einstein College of Medicine of Yeshiva
599 University for assistance in FRET. We thank Dr. Dangsheng Li for discussions and critical reading
600 of the manuscript. **Funding:** This work was supported by the National Key Research &
601 Development Program of China (2016YFC1303303, 2019YFA09003801, 2018YFA0900804), the
602 National Natural Science Foundation of China (31970685, 31671432, 81872314, 31770975,
603 81572799). **Author contributions:** Q.S. conceived the project and conception. Q.S., H.H. and J.L.
604 designed experiments with the advice from X.N.W. and Z.C.. J.L. performed majority of the
605 experiments with the assistance of X.Y. for RNA interference, phenotype and qPCR, and Z.N. for
606 pathology, immunostaining and FISH. M.W. B.Z. and H.Q helped in protein expression and
607 detection. S.G. and L.G. assisted imaging. Y.T. provided patient samples and related information.
608 Q.S., H.H. and J.L. analyzed the data with the assistance of Y.Z.. Q.S. and J.L. wrote the paper with
609 input from X.N.W, L.M. and H.H., and all authors reviewed the manuscript. **Competing interests:**
610 no conflict of interest to be stated.

611

612 **Figures**

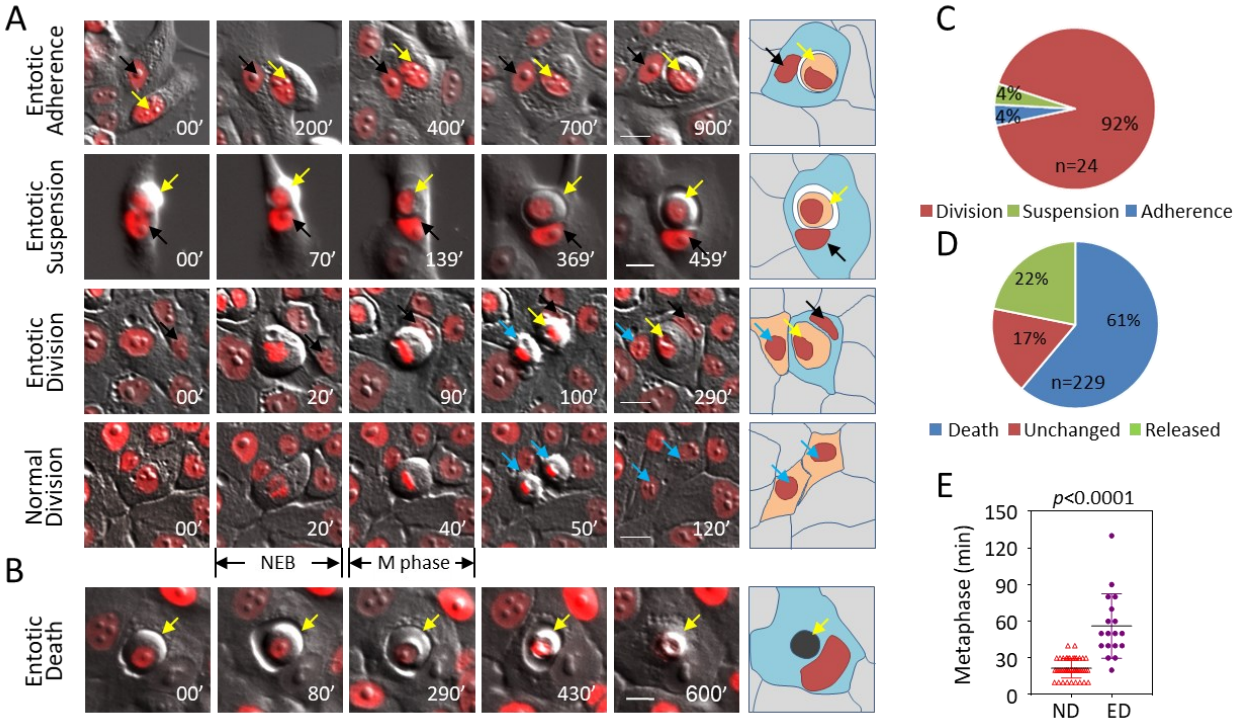

613
614 **Figure 1. Entosis is preceded by mitosis of prolonged metaphase.**

615 (A) Representative image sequences for the formation of entotic CIC structures from adherent cell (panel of
616 Entotic Adherence), suspended cells (panel of Entotic Suspension), divided cells (panel of Entotic
617 Division), and normal cell division (panel of Normal Division). Yellow arrows indicate internalized cells,
618 black arrows indicate outer cells, blue arrows indicate cells adhered to plate bottom. NEB: nuclear
619 envelop breakdown; Scale bar: 20 µm. Also see Movie S1.
620 (B) Representative image sequences for inner cell death of entotic CIC structures in MCF10A cells. Arrows
621 indicate inner cell. Scale bar: 20 µm.
622 (C) Quantification of Entotic Adherence (Adherence), Entotic suspension (Suspension) and Entotic Division
623 (Division). Quantification of inner cell fates in entotic CIC structures over 24 h period in MCF10A cells.
624 Also see Movie S3.
625 (D) Metaphase analysis of normal cell division (ND) and entotic cell division (ED) referring to cell division
626 leading to entotic CIC formation in MCF10A cells. n=52 for ND, 18 for ED.
627

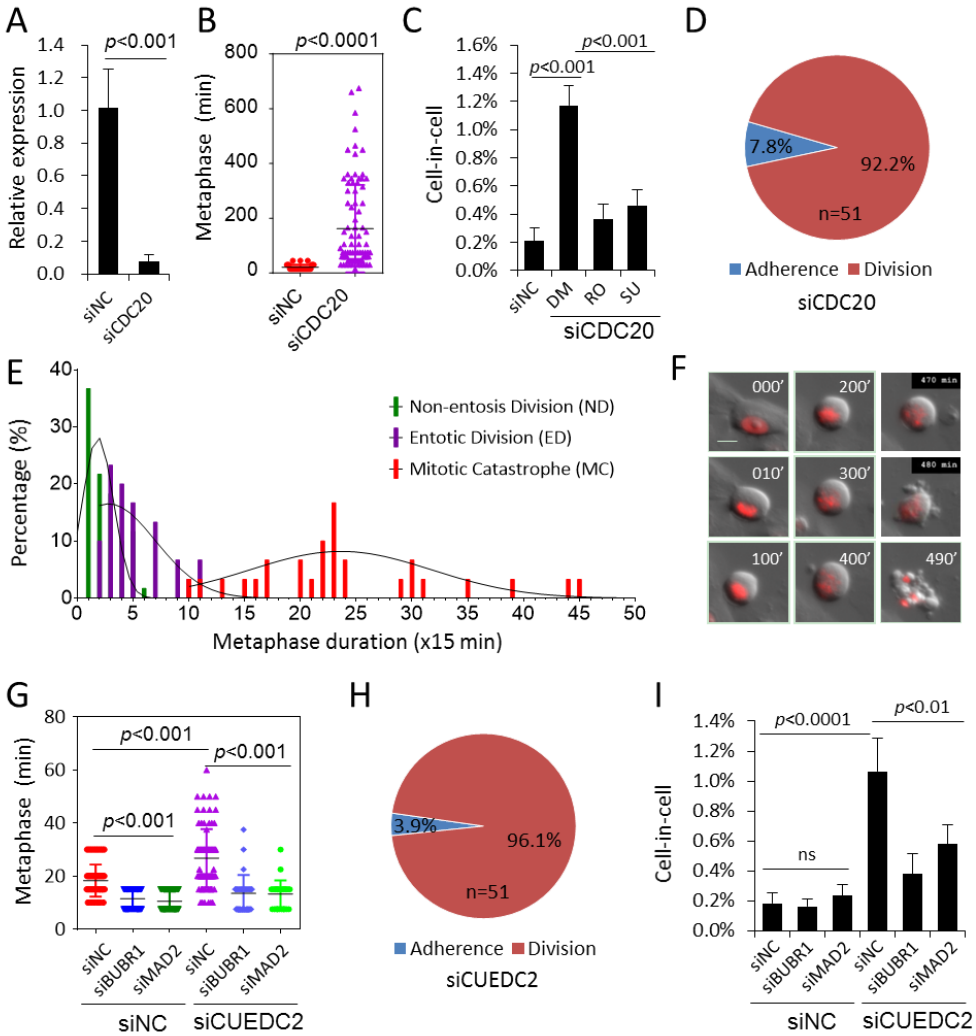

Figure 2. Prolonged mitosis primes cells to undergo entosis.

(A) CDC20 mRNA level examined by quantitative PCR (qPCR) upon knockdown by RNA interference. Data are mean ± SD of triplicate experiments. $p<0.001$.

(B) Graph plots metaphase duration of control (siNC, n=30) and CDC20 depleted (siCDC20, n=90) cells. $p<0.0001$.

(C) Quantification of CIC structures in control (siNC) and CDC20 (siCDC20) depleted cells. DM: DMSO; RO: Ro-3306(10 μM); SU: SU-9516 (5 μM. Data are mean ± SD of 4 or more fields with more than 5000 cells analyzed each. $p<0.001$ for the pairs of siNC vs DM, DM vs RO, DM vs SU.

(D) Quantification of Entotic Adherence (Adherence) and Entotic Division (Division) in MCF10A cells with CDC20 depletion.

(E) Histogram analysis with fitted curves of metaphase from non-entosis division (ND), entotic division (ED) and mitotic catasphrohpe (MC).n=30 for ND and MC, 24 for ED. Gaussian curve was created by nonlinear regression of the frequency distribution by GraphPad Prism software.

(F) Image sequence shows example of mitotic catastrophe with 490 min metaphase. Also see Movie S4. Scale bar: 20 μm

(G) Graph plots metaphase duration of control (siNC) and CUEDC2, BUBR1 and MAD2 depleted cells. From left to right, n=58, 60, 60, 85, 30, 30, respectively. $p<0.001$ between pairs analyzed as indicated.

(H) Quantification of Entotic Adherence (Adherence) and Entotic Division (Division) in MCF10A cells with CUEDC2 depletion.

(I) Quantification of CIC structures in cells co-depleting CUEDC2 with BUBR1 or MAD2 genes. Data are mean ± SD of 4 or more fields with more than 5000 cells analyzed each. ns: not significant. $p<0.0001$ between siCUEDC2 and siNCs, $p<0.01$ between siNC and siBUBR1 or siMAD2 within siCUEDC2 group.

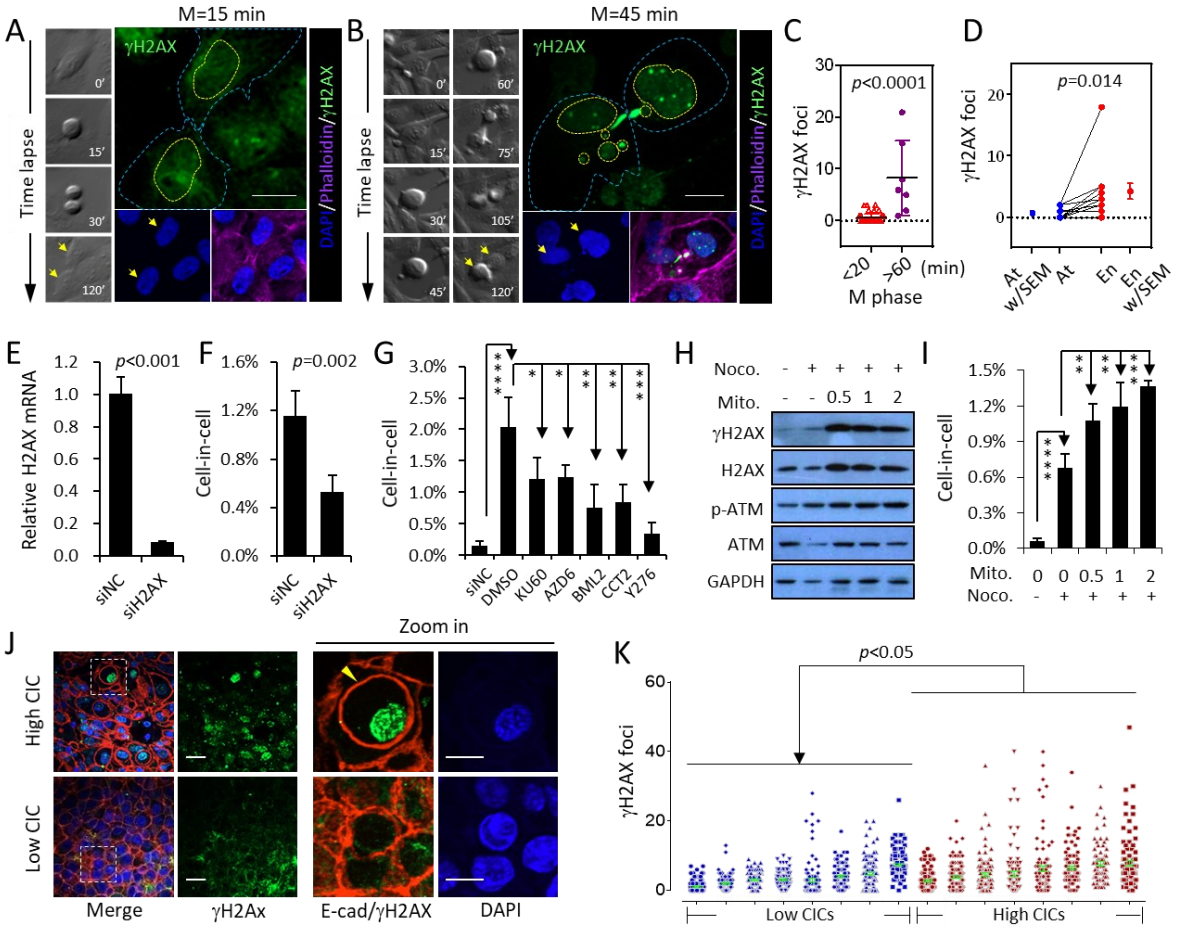

Figure 3. Mitotic DNA damages promote mintosis.

(A-B) Representative images for time lapse-associated immunostaining of γH2AX in mitotic cells of short M phase (A, 15 min) and long M phase (B, 45 min), with corresponding DIC images of time lapse on the left and images for DAPI and merge channels on the bottom. Arrows indicate sibling cells. Blue dashed lines depict cell shape, yellow dashed lines depict shape of nuclei. Note: sibling cells from long M phase (B, 45 min) contain micronuclei indicating chromosome missegregation, and multiple γH2AX foci indicating DNA damages. Scale bar: 10 µm.

(C) Number of nuclear γH2AX foci in cells from mitosis of different M phases. n=48 for M phase<20 min and 7 for M phase>60 min.

(D) Number of nuclear γH2AX foci in paired sibling cells with one attached to the culture bottom (At) while another internalized to form CIC structure (En). n=12.

(E-F) H2AX depletion (E) inhibits mintotic CIC formation (F). Data are mean ± SD of 4 or more fields with more than 5000 cells analyzed each.

(G) Effects of inhibiting DDR signaling on mintotic CIC formation in CUEDC2-depleted cells by compounds targeting ATM (KU60 for KU-60019), ATR (AZD6 for AZD6738), CHK1 (BML2 for BML-277) and CHK2 (CCT2 for CCT245737). Inhibition of ROCKs by Y27632 (Y276) as positive control. Data are mean ± SD of 4 or more fields with more than 4000 cells analyzed each. siNC for non-target control siRNA.

(H) DNA damages by mitomycin (Mito.) increase expression of γH2AX and phospho-ATM in cells synchronized in M phase by nocodazole (Noco.).

(I) Formation of mintotic CIC structures in cells 18 hours released from mitotic arrest under conditions in (H). Data are mean ± SD of 4 or more fields with more than 4000 cells analyzed each.

(J) Representative images for γH2AX staining in breast cancer tissues. E-cadherin (E-cad) in red indicates cell junctions. Arrow head indicates inner cell of a CIC structure. Scale bars: 20µm for the left, 10µm for zoomed images in the right.

(K) Quantification of nuclear γH2AX foci in 16 human breast cancer samples. About one hundred of cells were quantified for each sample.

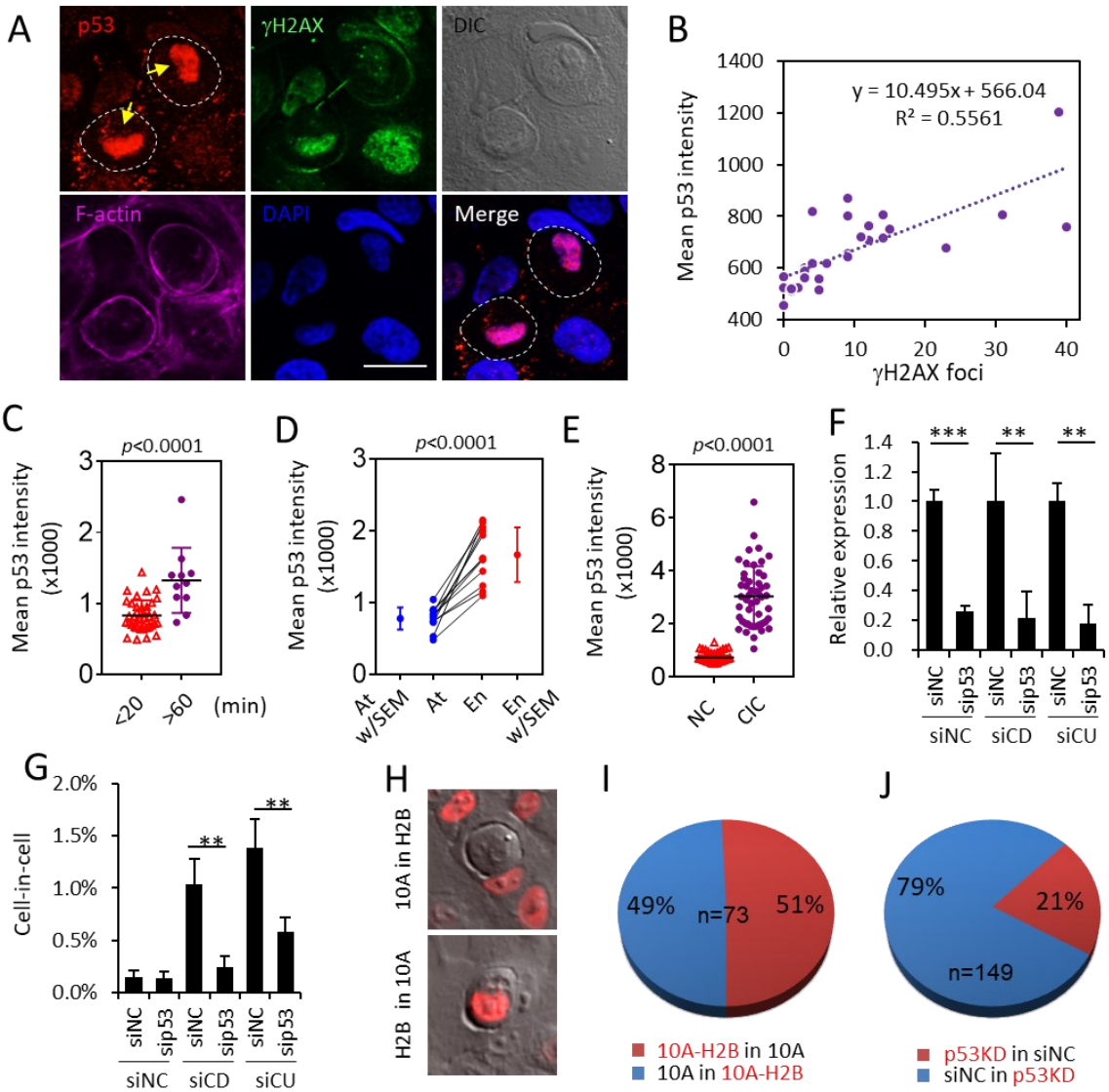

Figure 4 p53 signaling pathway is required for mintosis.

(A) Representative images for p53 staining in daughter cells forming CIC structures as indicated by yellow arrows. Scale bar is 10μm.

(B) Correlation analysis between p53 expression and number of nuclear γH2AX foci in MCF10A cells. n=30.

(C) Expression of p53 as indicated by mean staining intensity in cells from mitosis of different M phases. n=38 for M phase<20 min and 11 for M phase>60 min.

(D) Expression of p53 in paired sibling cells with one attached to the culture bottom (At) while another internalized to form CIC structure (En). n=12.

(E) Expression of p53 in inner cells of fresh CIC structures (CIC) is higher than that in single mono-nucleic cell (NC). n=50 for each group.

(F-G) p53 depletion (sip53) inhibits mintotic CIC formation induced by CDC20 (siCD) and CUEDC2 (siCU) knockdown. siNC for non-target control siRNA.

(H-J) Reduced frequency for p53 knockdown (p53KD) cells (labeled with H2B-mCherry in (J)) to penetrate into control cells (siNC). siNC for non-target control siRNA.

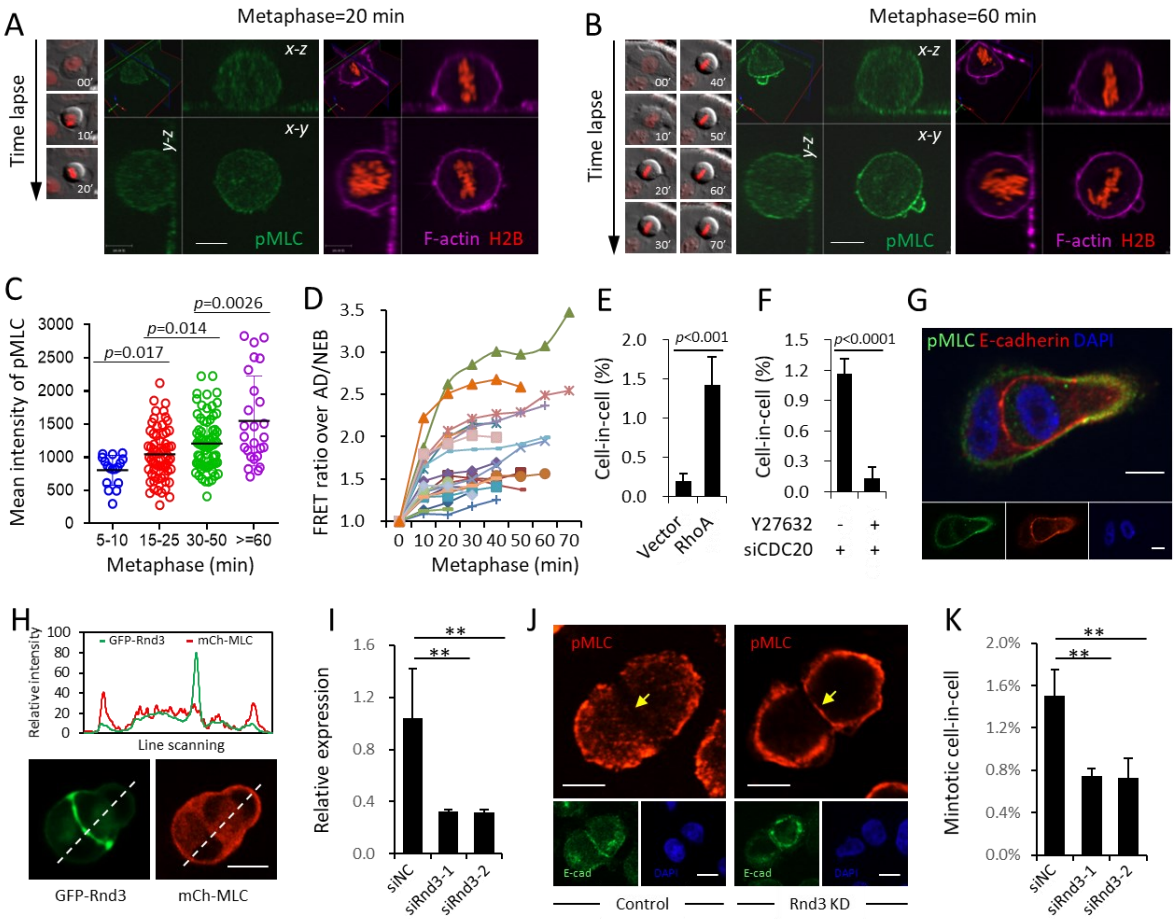

Figure 5. Rnd3 is required for asymmetric RhoA activation and mintotic CIC formation.

(A-B) Representative image of pMLC staining in mitotic cell of normal metaphase (20 min) (A) or prolonged metaphase (60 min) (B), with corresponding DIC/mCherry images of time lapse on the left and F-actin staining on the right. Scale bar: 10 µm. Also see Movie S5.

(C) Graph plots pMLC mean intensity in mitotic cells of different metaphase duration as indicated. From left to right, n=17, 67, 75, 26, respectively. Mean pMLC intensity of individual cell was calculated by normalization of background-subtracted pMLC intensity over cell area. Data are mean ± SD of 20 fields with totally more than 10 thousands of cells analyzed.

(D) The RhoA activity dynamics over metaphase measured by FRET analysis in 21 mitotic cells depleting CDC20. All background-subtracted mean FRET intensities were normalized over their corresponding mean FRET intensities at the time points of nuclear envelop breakdown (NEB) or cell adherence (AD) right before rounding up, whichever applied. Cn refers to different cell analyzed. Also see Movie S6.

(E) Quantification of CIC structures in cells overexpressing RhoA. Data are mean ± SD of 4 or more fields with more than 3000 cells analyzed each. $p<0.001$.

(F) Inhibition of CIC formation in CDC20 depleted cells by Y27632, a ROCKs inhibitor that blocks RhoA signaling. Data are mean ± SD of 4 or more fields with more than 5000 cells analyzed each. $p<0.0001$.

(G) Polarized distribution of pMLC at the rear cortex of internalized cell in intermediate CIC structure. Scale bars: 10 µm. Also see Figure S4E.

(H) Rnd3-GFP localizes at the cell-cell junction during CIC formation. Upper graph shows line scan analysis, channeled images were shown underneath. Scale bar: 10 µm.

(I) Rnd3 mRNA level examined by quantitative PCR (qPCR) upon knockdown by RNA interference. Data are mean ± SD of triplicate experiment. $p<0.001$.

(J) Representative images for junctional localization of pMLC2 (red) MCF10A cell doublets (right panel) upon Rnd3 depletion (Rnd3 KD), E-cadherin (green) staining indicates cell junctions. Scale bars: 10 µm. Arrowheads indicate pMLC2 staining at cell junctions. Also see Figure S4G

(K) Quantification of mintotic CIC formation in control (siNC) and Rnd3 (siRnd3) depleted cells. data are mean ± SD of 4 or more fields with more than 5000 cells analyzed each. $p<0.01$.

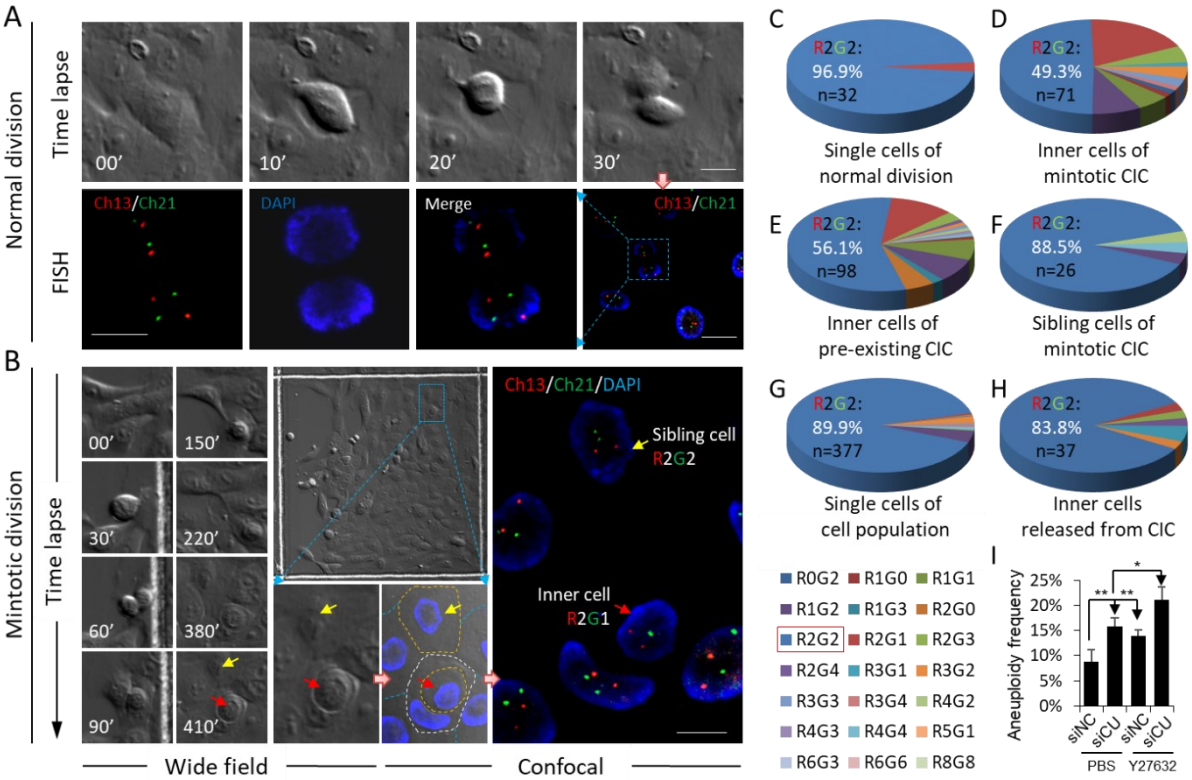

Figure 6. Mintosis selectively targets non-diploid cells for CIC-mediated death.

(A) Representative images showing FISH result of normal cell division. Upper panel shows DIC image sequence of time lapse. Lower panel shows FISH results in two daughter cells. Scale bar: 20 μm for right, 10 μm for left. Also see Movie S7.

(B) Representative images showing FISH result of cell division leading to CIC formation. Left panel shows DIC image sequence of time lapse. Middle panel shows the positional information of target cells/structures in gridded glass bottom dish at the end of time lapse imaging. Right panel shows FISH results of selected region in middle panel. Scale bar: 10 μm. Yellow arrow indicates adherent sibling daughter cell, red arrow indicates daughter cell internalized to form CIC structure. FISH results are presented as RnGn, R for red probe, G for green probe, n for probe number. Also see Movie S7.

(C-H) Detail quantification and classification of FISH results for daughter cells of normal division with metaphase not more than 30 min (C), daughter cells from cell division that were internalized to form CIC structures (D), inner cells of pre-existing CIC structures of unknown origin (E), daughter cells from cell division that did not form CIC structures (F), single cells of unknown origin in the cell population (G), and internalized cells that were finally released from CIC structure (H), see Figure S5B and Movie S7. FISH results are presented as RnGn, R for red probe, G for green probe, n for probe number. The percentage of R2G2 together with cell number analyzed were shown for each pie picture. The related histories for all cells analyzed were determined by time lapse imaging.

(I) Quantification of non-diploid cells following mintosis blockade. siNC: non-target control siRNA; siCU: siRNA for CUEDC2. “*” for $p<0.05$; “**” for $p<0.01$. For each condition, quantification was performed on >400 cells..

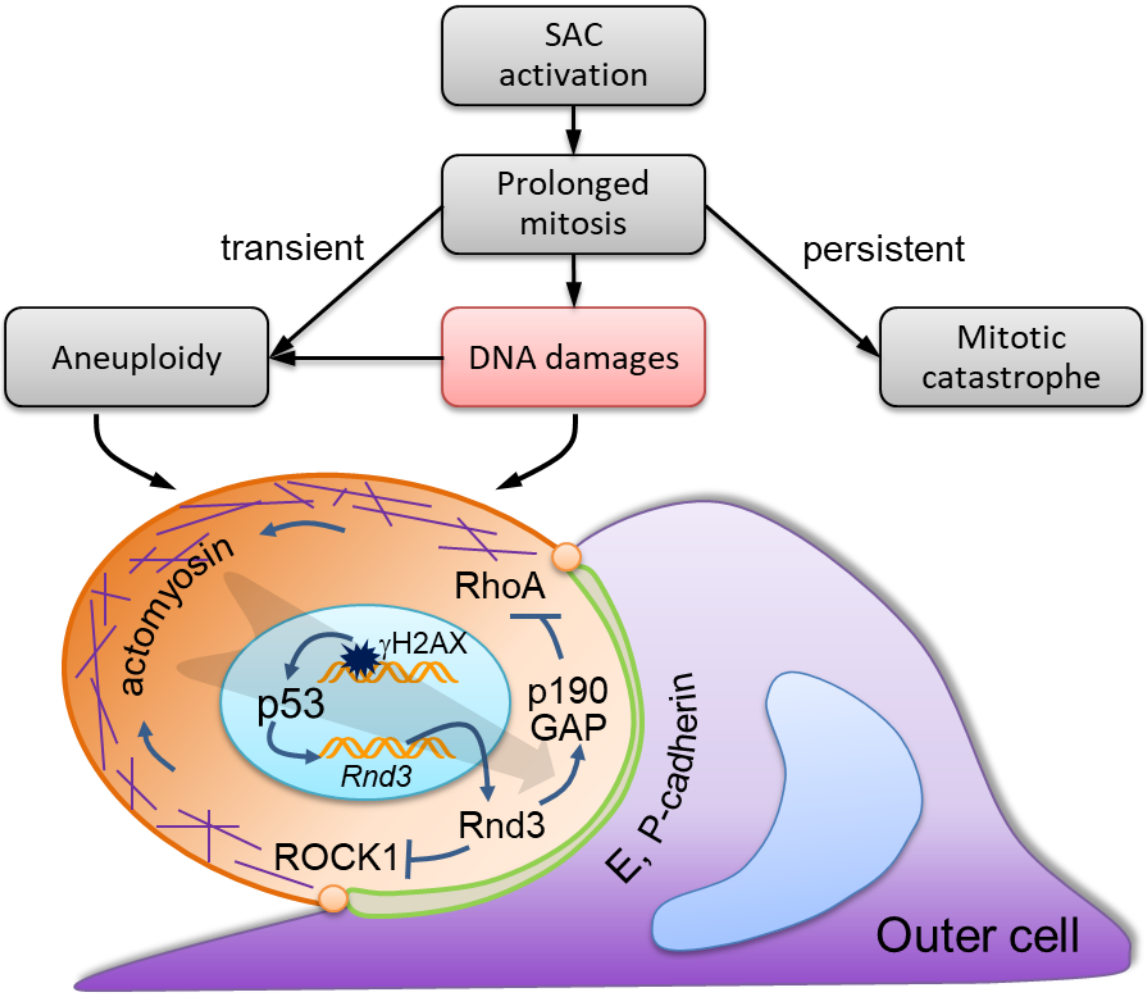

Figure 7. Working model for p53-depedent postmitotic surveillance by mintosis.

SAC activation leads to mitotic arrest characterized by prolonged metaphase. While persistent mitotic arrest activates cell death by mitotic catastrophe prior to cytokinesis, transient mitotic arrest may cause DNA damages that promote chromosome missegregation to give rise to daughter cells of aneuploidy. DNA damages marked by gH2AX activate DDR signaling and p53 in daughter cells. p53 upregulates the expression of downstream target Rnd3 which, by targeting ROCK1 and p190 RhoGAP, inhibits RhoA activities at cell-cell junction where lie E-, P-cadherin, leading to polarized activation of RhoA-actomyosin at rear cortex which drives cell internalization to form CIC structures. Subsequent death promoted by the outer cell eliminates those aneuploid daughter cells to maintain genome integrity.

764 **Supplementary Materials**

765

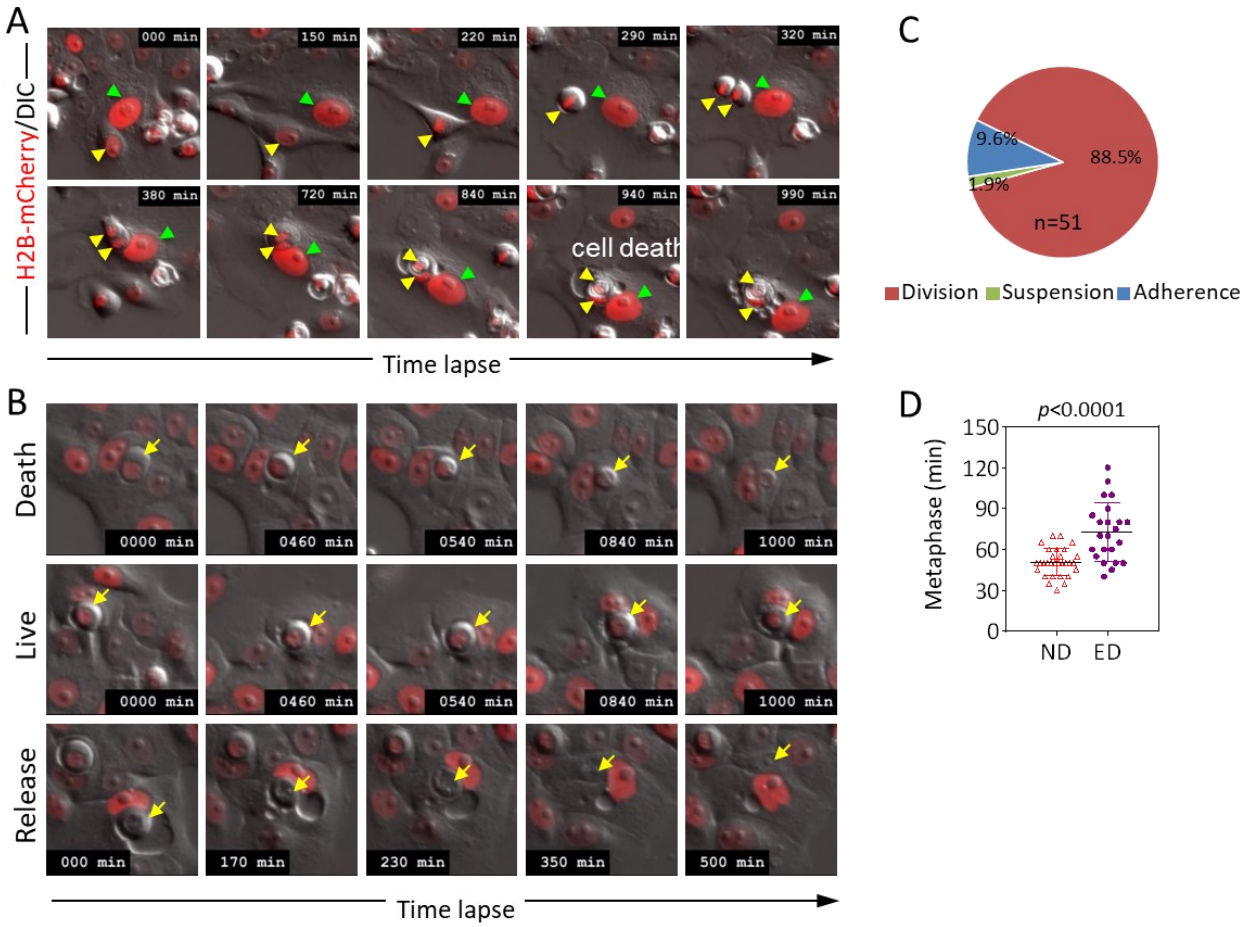

766

767

768 **Figure S1. Entosis is coupled with mitotic cell division. Related to Figure 1.**

769 (A) Image sequence shows the process of entotic cell-in-cell formation and inner cell death following mitotic cell
770 division in MCF10A/H2B-mCherry cells. Yellow arrows indicate cells undergoing mitosis and
771 internalization, green arrows indicate outer cells.
772 (B) Representative image sequences of different inner cell fates for entotic cell-in-cell structures of MCF10A
773 cells. Arrows indicate inner cells. Also see Movie S2.
774 (C) Quantification of three ways leading to CIC structures in MCF7 cells. n=51.
775 (D) Metaphase analysis of normal cell division (ND) and entotic cell division (ED) referring to cell division
776 leading to entotic CIC formation in MCF7 cells. n=30 for ND, 23 for ED. $p<0.0001$.

777

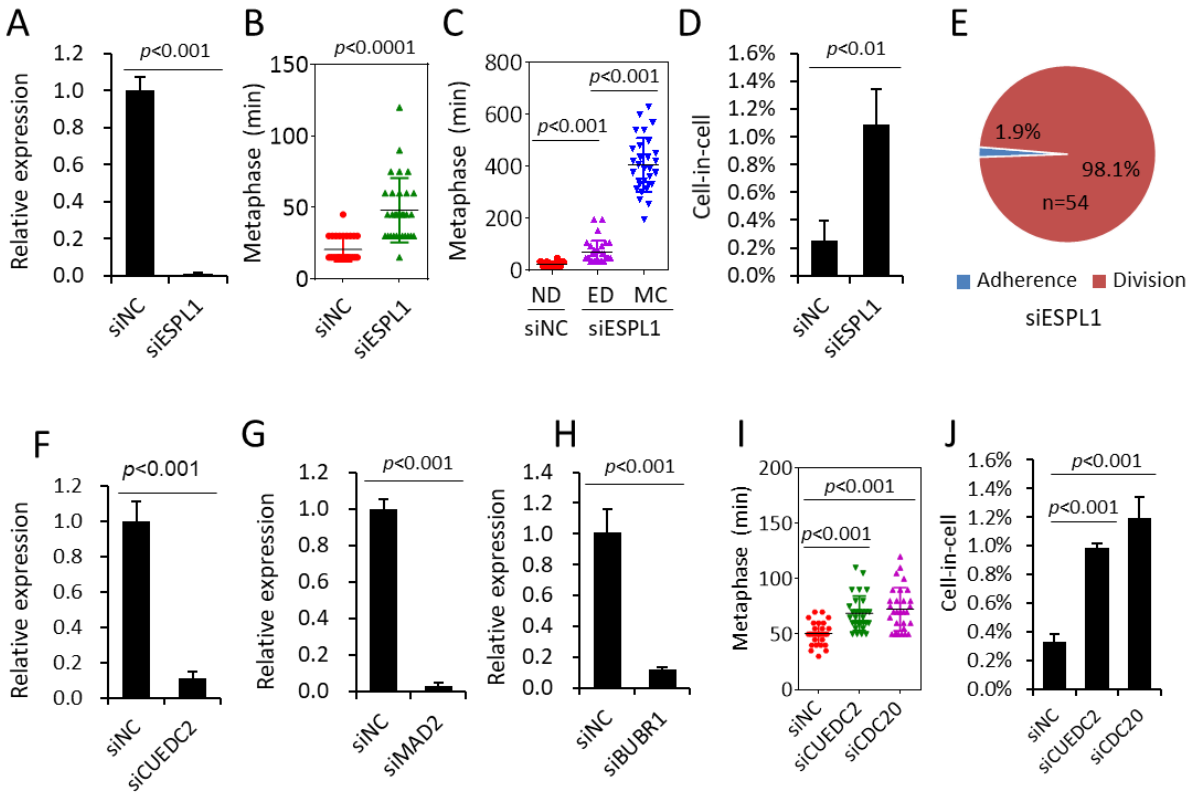

Figure S2. Prolonged mitosis primes cells to undergo entosis. Related to Figure 2.

(A) ESPL1 mRNA level examined by quantitative PCR (qPCR) upon knockdown by RNA interference. Data are mean ± SD of triplicate experiment. $p<0.001$.

(B) Quantification of CIC structures in control (siNC) and ESPL1 (siESPL1) depleted cells. Data are mean ± SD of 4 or more fields with more than 5000 cells analyzed each. $p<0.01$.

(C) Graph plots metaphase duration of control (siNC, n=30) and ESPL1 depleted (siESPL1, n=30) cells that didn't undergo entosis or mitotic catastrophe. $p<0.0001$.

(D) Quantification of CIC formation in control (siNC) and ESPL1 depleted (siESPL1) cells. Data are mean ± SD of 4 or more fields with more than 5000 cells analyzed each. $p<0.01$.

(E) Quantification of Entotic Adherence (Adherence) and Entotic Division (Division) in MCF10A cells with ESPL1 depletion.

(F) CUEDC2 mRNA level examined by quantitative PCR (qPCR) upon knockdown by RNA interference. Data are mean ± SD of triplicate experiment. $p<0.001$.

(G) MAD2 mRNA level examined by quantitative PCR (qPCR) upon knockdown by RNA interference. Data are mean ± SD of triplicate experiment. $p<0.001$.

(H) BUBR1 mRNA level examined by quantitative PCR (qPCR) upon knockdown by RNA interference. Data are mean ± SD of triplicate experiment. $p<0.001$.

(I) Graph plots metaphase duration of control (siNC) and CDC20 and CUEDC2 depleted (siCDC20, siCUEDC2) MCF7 cells. n=30 for each. $p<0.001$.

(J) Quantification of CIC structures in control (siNC) and CDC20 and CUEDC2 depleted (siCDC20, siCUEDC2) MCF7 cells. Data are mean ± SD of 4 or more fields with more than 5000 cells analyzed each. $p<0.001$.

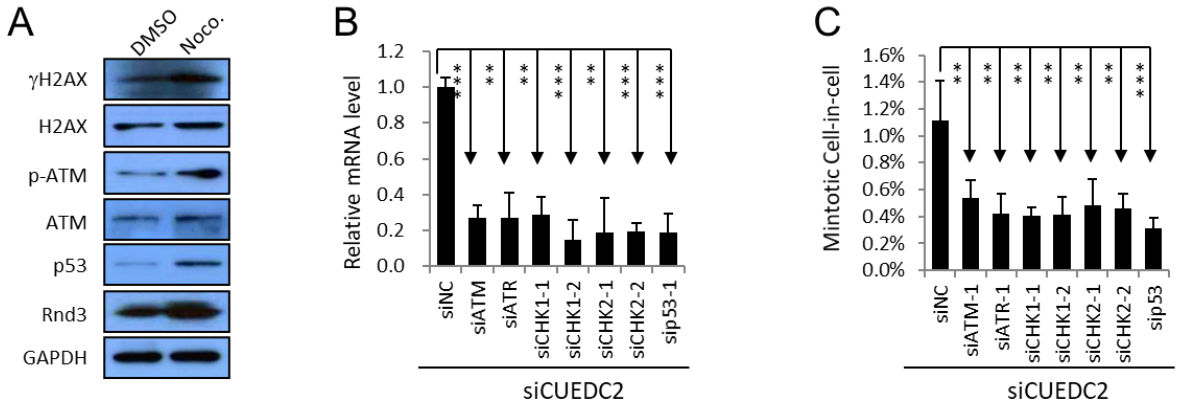

Figure S3. Involvement of DNA damage pathway in mintosis. Related to Figure 3.

(A) Activation of DNA damage response (DDR) signaling during mitotic arrest. Expression of genes of DDR pathway in nocodazole (Noco.)-treated MCF10A cells were detected by Western blot.

(B) mRNA levels of genes in DDR pathway examined by quantitative PCR (qPCR) upon knockdown by RNA interference. Data are mean ± SD of triplicate experiment. $p<0.001$.

(C) Decreased mintotic CIC formation in MCF10A cells upon depletion of genes in DDR pathway by RNA interference. Data are mean ± SD of 4 or more fields with more than 5000 cells analyzed each. "**" for $p<0.01$; "***" for $p<0.001$.

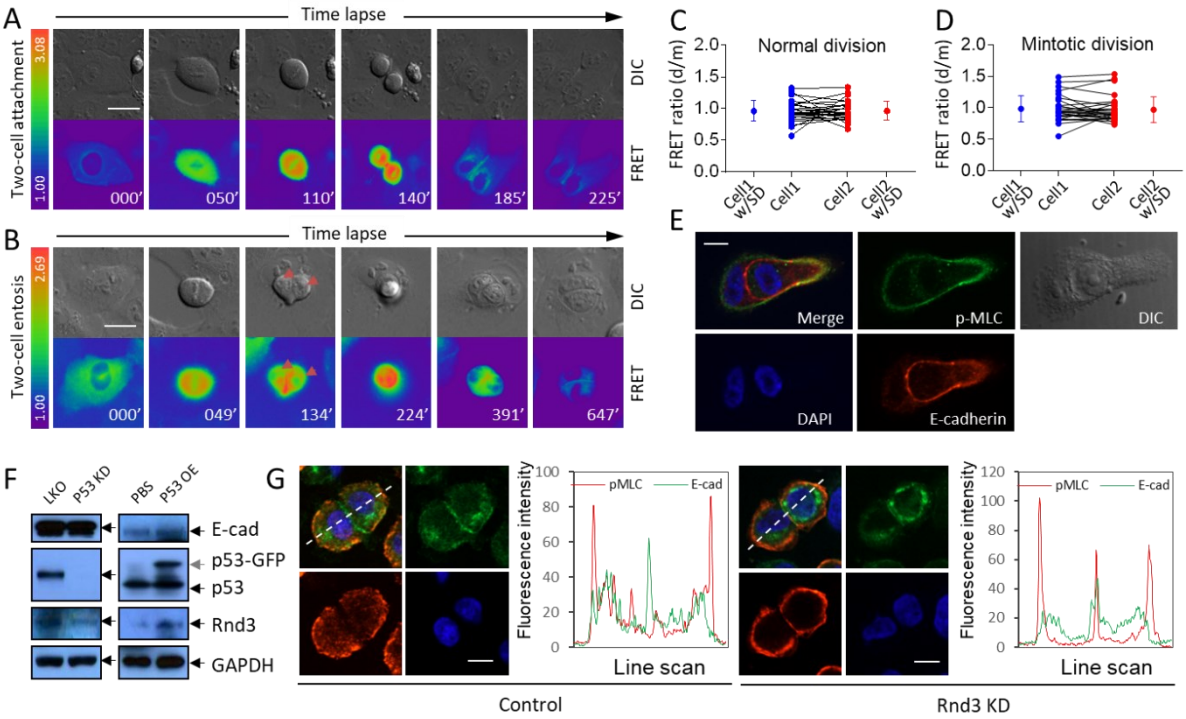

Figure S4. Compartmentalized RhoA activity by Rnd3 is required for mintosis. Related to Figure 5.

(A) Representative FRET image sequence shows RhoA activity changes during cell division with two daughter cells attached to plate bottom. Scale bar: 20 µm.

(B) Representative FRET image sequence shows RhoA activity changes in cell division with two daughter cells internalized to form CIC structures. Scale bar: 20 µm.

(C-D) RhoA FRET ratios between daughter cells right after cytokinesis (d) and their respective mother cells in the end of metaphase (m) in normal cell division (C, n=28) and mintotic cell division (D, n=29).

(E) Representative images for polarized distribution of pMLC at the rear cortex of internalized cell in intermediate CIC structure. Scale bars: 10 µm. Identical to Figure 5G.

(F) Regulation of Rnd3 expression by p53 in MCF10A cells. Left panel shows decreased Rnd3 expression upon stable p53 knockdown (p53 KD) as compared with control (LKO). Right panel shows increased Rnd3 expression upon p53-GFP overexpression (p53OE).

(G) Representative images for junctional localization of pMLC (red) MCF10A cell doublets (right panel) upon Rnd3 depletion (Rnd3 KD), E-cadherin (green) staining indicates cell junctions. Scale bars: 10 µm. Arrowheads indicate pMLC staining at cell junctions. Related to Figure 5J.

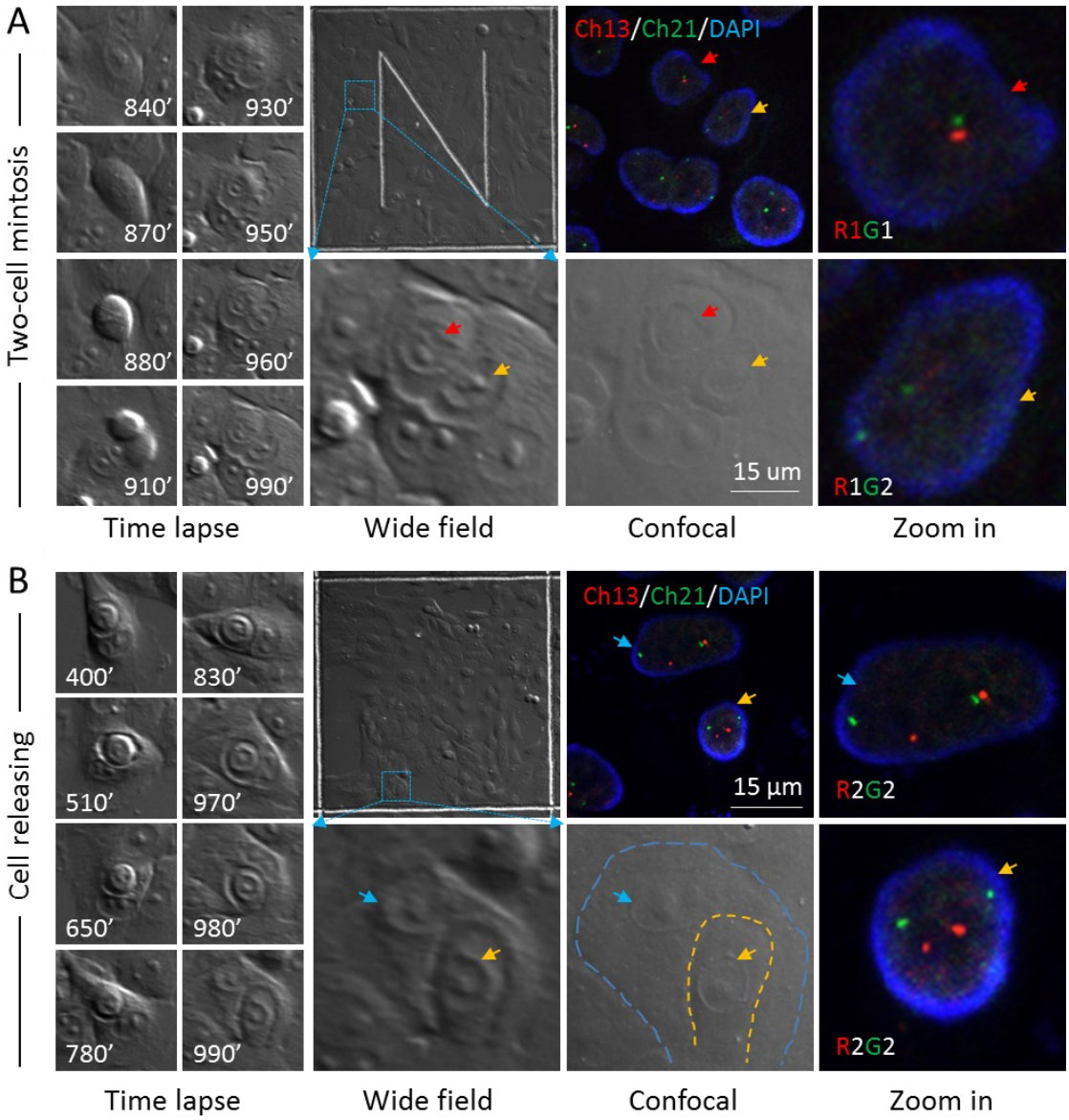

Figure S5. Mintosis selectively targets non-diploid cells for elimination. Related to Figure 6.

(A) Representative images showing FISH result of cell division leading to internalization of two daughter cells to form CIC structures. Left panel shows DIC image sequence of time lapse. Middle panel (wide field) shows the positional information of target cells/structures in gridded glass bottom dish at the end of time lapse imaging. Right panels (confocal and zoom in) show FISH results of selected region in middle panel. Scale bar: 15 µm. Yellow and red arrows indicate two daughter cell internalized. FISH results are presented as RnGn, R for red probe, G for green probe, n for probe number. See Movie S7.

(B) Representative images showing FISH result of cell releasing from CIC structures. Layout is same as that of (A). Scale bar: 15 µm. Yellow arrow indicates inner cell that is being released. Blue arrow indicates outer cell. FISH results are presented in the same way as (A). See Movie S7. Related to Figure 6H.

842 **Movie S1. The formation of entotic CIC structures.**
843 **Entotic Adherence:** MCF10A cell indicated by arrows penetrates into one of its neighboring cells
844 to form CIC structure while being adherent to matrix.
845 **Entotic Suspension:** Two MCF10A cells indicated by arrows likely first formed CIC structure
846 while being suspended, and then penetrated into one of their neighboring cells to form CIC
847 structure.
848 **Entotic Division:** Arrow indicated MCF10A cell first underwent cell division with a metaphase of
849 80 min, and then one of the daughter cells internalized into its neighboring cell to form CIC
850 structure.
851 **Normal Division:** Normal cell division with a short metaphase of 20 min and two daughter cells
852 adherent to matrix rapidly.
853
854 **Movie S2. Entosis is coupled with mitotic cell division.**
855 Yellow arrows-indicated cell underwent mitotic cell division, followed by internalization of two
856 daughter cells into their neighboring cell (green arrow). The most inner cell died prior to the end
857 of the time lapse.
858
859 **Movie S3. Inner cell fates in CIC structures.**
860 **Death:** Arrow indicated inner cell of a CIC structure died inside another MCF10A cell.
861 **Unchanged:** Arrow indicated inner cell of a CIC structure stayed alive inside another MCF10A
862 cell to the end of time lapse of 24 h.
863 **Released:** Arrow indicated inner cell initially resided in the vacuole of a CIC structure, then came
864 out alive as indicated by arrows.
865
866 **Movie S4. Catastrophic cell death of mitosis.**
867 CDC20 depleted mitotic MCF10A cell underwent prolonged metaphase of 480 min and finally
868 died in a catastrophic way.
869
870 **Movie S5. Mitosis of different metaphase.**
871 **M=20 min:** Mitotic MCF10A cell underwent short metaphase of 20 min.
872 **M=60 min:** Mitotic MCF10A cell with CDC20 depleted underwent prolonged metaphase of 60
873 min.
874
875 **Movie S6. RhoA activity by FRET during one-cell mintosis.**
876 RhoA activity by FRET in CDC20 depleted MCF10A cell first accumulated during metaphase,
877 then, one of the daughter cells that demonstrated delayed RhoA activity attenuation penetrated
878 into its neighboring cell to form CIC structure, while the daughter cell that rapidly reduced its
879 RhoA activity attached to plate bottom. Left is FRET channel, right is DIC channel.
880
881 **Movie S7. Time lapse for FISH.**
882 **Normal division:** Cell divided with metaphase less than 20 min, two daughter cells attached to
883 plate bottom shortly after division.
884 **Mintotic division:** Cell divided with one of the two daughter cells internalized to form CIC
885 structure at the end of time lapse, while another daughter cell attached to plate bottom shortly after
886 division.
887 **Two-cell mintosis:** Cell divided with both of the two daughter cells internalized to form CIC
888 structure at the end of time lapse.
889 **Inner cell releasing:** The arrow indicated inner cell of a CIC structure started to come out at the
890 end of time lapse.
891